THE JOURNAL OF PHYSICAL CHEMISTRY A

Article

pubs.acs.org/JPCA

Global Analytical Potential Energy Surface for the Electronic Ground State of NH_3 from High Level ab Initio Calculations

Roberto Marquardt*

Laboratoire de Chimie Quantique, Institut de Chimie UMR 7177 CNRS/Université de Strasbourg, 1 rue Blaise Pascal, BP 296/R8, Strasbourg CEDEX, France

Kenneth Sagui

Laboratoire de Chimie Theorique, Université de Marne-la-Vallée 5 Bd Descartes (Champs-sur-Marne), F-77454 Marne-la-Vallée Cedex 2, France

Jingjing Zheng and Walter Thiel

Max-Planck-Institut für Kohlenforschung, Kaiser-Wilhelm-Platz 1, D-45470 Mülheim an der Ruhr, Germany

David Luckhaus

Chemistry Department, University of British Columbia, 6174 University Boulevard, Vancouver, BC V6T 1Z3, Canada

Sergey Yurchenko

Department of Physics and Astronomy, University College London, London, WC1E 6BT, U.K.

Fabio Mariotti and Martin Quack

Laboratorium für Physikalische Chemie, ETH Zürich Wolfgang Pauli Str. 10, CH-8093 Zürich, Switzerland

Supporting Information

ABSTRACT: The analytical, full-dimensional, and global representation of the potential energy surface of NH_3 in the lowest adiabatic electronic state developed previously (Marquardt, R.; et al. *J. Phys. Chem. B* **2005**, *109*, 8439−8451) is improved by adjustment of parameters to an enlarged set of electronic energies from ab initio calculations using the coupled cluster method with single and double substitutions and a perturbative treatment of connected triple excitations (CCSD(T)) and the method of multireference configuration interaction (MRCI). CCSD(T) data were obtained from an extrapolation of aug-cc-pVXZ results to the basis set limit (CBS), as described in a previous work (Yurchenko, S.N.; et al. *J. Chem. Phys* **2005**, *123*, 134308); they cover the region around the NH_3 equilibrium structures up to 20 000 hc cm^{-1}. MRCI energies were computed using the aug-cc-pVQZ basis to describe both low lying singlet dissociation channels. Adjustment was performed simultaneously to energies obtained from the different ab initio methods using a merging strategy that includes 10 000 geometries at the CCSD(T) level and 500 geometries at the MRCI level. Characteristic features of this improved representation are NH_3 equilibrium geometry $r^{eq}(NH_3) \approx 101.28$ pm, $\alpha^{eq}(NH_3) \approx 107.03°$, the inversion barrier at $r^{inv}(NH_3) \approx 99.88$ pm and 1774 hc cm^{-1} above the NH_3 minimum, and dissociation channel energies 41 051 hc cm^{-1} (for $NH_3 \rightarrow (^2B_2)NH_2 + (^2S_{1/2})H$) and 38 450 hc cm^{-1} (for $NH_3 \rightarrow (^3\Sigma^-)NH + (^1\Sigma_g^+)H_2$); the average agreement between calculated and experimental vibrational line positions is 11 cm^{-1} for $^{14}N^1H_3$ in the spectral region up to 5000 cm^{-1}. A survey of our current knowledge on the vibrational spectroscopy of ammonia and its isotopomers is also given.

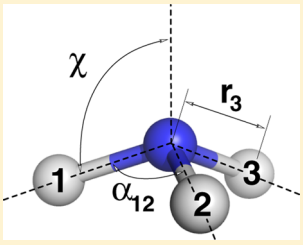

1. INTRODUCTION

Multidimensional, analytical representations of potential energy surfaces (PES) are ideally useful to understand the often complex structure and dynamics of polyatomic molecules. Currently, representations are based on multivariate interpolation approaches, multidimensional polynomial expansions, and specially devised, analytical functional forms (see refs 1−5 and references cited therein). Interpolation methods give exact representations of the original ab initio data used to determine the PES, while

Special Issue: Joel M. Bowman Festschrift

Received: February 17, 2013
Revised: May 20, 2013
Published: May 20, 2013

polynomial or other analytical functional forms may be used within a least-squares fitting algorithm to adjust the representation either to ab initio data of the PES or to experimentally available, derived properties of the PES, such as the position of spectral lines, transition intensities, reactive scattering cross-sections or thermochemical data. Sometimes both ab initio and experimental data are used together to develop realistic analytical representations, such as for methane,[5−8] hydrogen peroxide,[9] water,[10] $(HF)_2$,[11−13] and ammonia, in particular.[14−17]

Of particular interest are *global* analytical representations of PES that are defined in the entire configuration space because such representations can be used to describe both small and large amplitude motions of atoms within a one-piece modeling of the adiabatic interactions of atoms in molecules. Such representations may for instance be derived from accurate, high-resolution spectroscopic data and may provide a similarly accurate basis for quantum dynamical calculations of scattering processes. The derivation of realistic, global analytical representations of PES has become a somewhat standard procedure for molecular systems up to three atoms,[10,18−21] but it is considerably more difficult for systems with more than three atoms, where more than one valence bond angle exists, and realistic representations of this kind are consequently rare. A few examples of global analytical representations for covalently bonded tetra- to hexa-atomic molecules have been developed in the last years,[7,8,22,23] among which we wish to emphasize here the work of J. M. Bowman and his group.[4,24−28]

Key characteristic elements of appropriate global analytical representations of PES are the *robustness* to small changes of parameter values, the *flexibility* in describing a large set of data originating from quite different sources, and the *compactness*, i.e., the property of depending on a rather small number of parameters, while offering a satisfactory degree of flexibility. An example for a global PES representation that (almost) satisfies these criteria is the Morse potential for a diatomic molecule.[29] Our previous work on methane[7,8] and ammonia PES[22] provides examples of rather compact representations of PES for polyatomic molecules.

Describing the adiabatic ground state PES of ammonia analytically has the additional difficulty imposed by the existence of a conical intersection seam for planar ammonia molecules in the region of the single bond dissociation channels

$$NH_3(^1A_1) \rightarrow NH_2(^2B_1) + H(^2S_{(1/2)}) \quad (1)$$

and

$$NH_3(^1A_1) \rightarrow NH_2(^2A_1) + H(^2S_{(1/2)}) \quad (2)$$

The $\tilde{X}^1A_1$ state of NH_3 correlates diabatically with the energetically higher $^2A_1$ state of NH_2 in eq 2, whereas the first excited singlet state ($\tilde{A}^1A_2''$) of ammonia correlates diabatically with the $^2B_1$ channel. An analytical representation of a single adiabatic PES sheet in the conical intersection seam is strictly impossible because of the occurrence of cusp singularities. Studies on the four-dimensional conical intersection seam of ammonia and the nonadiabatic couplings have been reported.[30−32] In refs 31 and 33, a two-sheet analytical representation of the lowest adiabatic electronic states of ammonia is derived from a direct calculation of diabatic states. In ref 34, a three-sheet analytical representation for the ammonia cation is deduced from a different diabatization ansatz. Recent reports address new representations for the diabatic $\tilde{X}$ and $\tilde{A}$ states of ammonia[32] and a potential energy representation for the first excited triplet state from a double many-body expansion.[35]

Following our previous work, we adopt here the point of view that adiabatic or diabatic representations of molecular *states* including both nuclear and electronic degrees of freedom are anyway inappropriate representations of molecular eigenstates in regions close to conical intersection seams and that the nuclei will move on the lowest adiabatic PES, while approaching to and departing from the regions defining a conical intersection, whenever their kinetic energy is sufficiently small compared to the coupling energy given by the nonadiabatic terms neglected in the Born−Oppenheimer approximation or other neglected coupling terms. For instance, while nonadiabatic terms vanish by symmetry at planar geometries of ammonia,[31] additional couplings arising from spin−orbit interaction might be important, due to the vicinity of the spin-forbidden reaction channel

$$NH_3(^1A_1) \rightarrow NH(^3\Sigma^-) + H_2(^1\Sigma_g^+) \quad (3)$$

which is actually the lowest dissociation channel of ammonia. We therefore describe the lowest adiabatic PES of ammonia with a single-valued analytical representation. Within such a representation, the region pertaining to a conical intersection is modeled with smooth functions, rather than cusps. Those functions might give rise to local maxima in low-dimensional sections of the potential energy hypersurface. This is in contrast to diabatic representations, which will behave rather monotonically in the regions pertaining to conical intersection seams. The latter are, when used as single-valued representations of the potential energy surfaces, poor representations of the spectroscopic states in regions that are distant from conical intersection seams. As we consider in this work single-valued representations that should also be appropriate for the spectroscopy of all reactants and products in all reaction channels, we use the adiabatic representation.

In a previous work,[22] a PES called AMMPOT2 was obtained from ab initio data obtained at the CASPT2 level. While the overall agreement with experimental results is qualitatively satisfactory for AMMPOT2, it is less good quantitatively. An improvement could be achieved by using ab initio data obtained at a higher level of theory. Very accurate data for ammonia have become available at the ic-ACPF[36] and the CCSD(T) level, the latter at the basis set limit.[37−40] These data were used to set up PES representations for ammonia. For the CCSD(T) data, these representations are locally defined around the two pyramidal minimum structures by means of polynomial expansions. Those representations were used to calculate vibrational term values and transition dipole moments that agree very well with experimental data from high resolution spectroscopy. The high accuracy of the theoretical vibrational term values is related to the high level of flexibility of the polynomial representations, which allow them to describe extremely well data from highly accurate ab initio calculations; this is the great advantage of using polynomial expressions. It should be noted that, despite the accuracy of the calculations, which include even nonadiabatic corrections,[16] the currently best available representations of the potential energy surfaces of ammonia make use of an experimental refinement during the adjustment of parameters.[14,16,17] Important drawbacks of polynomial expansions are, first, that they are not global because the CCSD(T) data, for example, have a local definition range: it was shown[22] that indeed the data from ref 38 correlate asymptotically with the $^2A_1$ channel. Second, those representations are not sufficiently compact because of the rather long polynomial expansion used.

In the present work, we explore the possibility of combining the highly accurate data available at the CCSD(T) level with

dx.doi.org/10.1021/jp4016728 | J. Phys. Chem. A 2013, 117, 7502−7522

accurate data obtained by MRCI calculations that account for the change of electronic configuration along the dissociation channels. The idea is to follow a *merging* strategy of ab initio data in order to build up a single set of energy data points that can be used to fit a global, yet accurate PES for ammonia.

We present a new, global, and compact representation of the PES for the adiabatic ground state of ammonia. The representation is further analyzed with respect to its key topographical properties, and vibrational eigenstates up to 10 000 cm^{-1} are determined from a full-dimensional variational calculation. Results are discussed in relation to the thermochemistry and spectroscopy of ammonia. Comparison is made with results obtained in previous work on the PES and spectroscopy of ammonia.[14,16,17,36−39,41−43] In particular, we give an overview of current state-of-the-art experimental and theoretical vibrational spectroscopic data including transition line positions and cross-sections up to 15 000 cm^{-1} for ammonia and transition line positions up to 5000 cm^{-1} for some isotopomers. It should be noted that, despite its rather good flexibility, the analytical function developed in this work cannot compete with polynomial representations such as in refs 36 and 38 in terms of accuracy in the prediction of ro-vibrational term values. The latter can nevertheless be described well enough to guarantee a physically sound description of complete reactive processes occurring on the potential energy surface.

In order to label the different PES representations discussed in this article, acronyms are used as defined in ref 22. In addition, we discuss results from ref 36 as well as refs 16 and 43, which are given the acronyms HSL-0 and HSL-2 PES, respectively, as well as results from the evaluation of the CBS**4 PES representation from ref 38, which is called YZLJT PES here. Figure 1 shows a picture of NH_3 with the coordinate definitions used in this work.

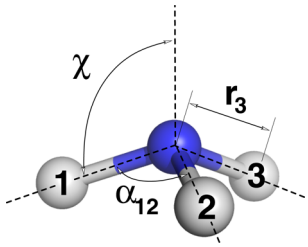

Figure 1. Representation of the ammonia molecule with coordinate definitions used in this work; the analytical representation is set up as a multidimensional function of the bond lengths r_i and bond angles α_{ij} (only r_3 and α_{12} are indicated, for convenience); the inversion angle χ is used in some of the graphical representations shown below.

2. THEORY

2.1. Ab Initio Calculations. The CCSD(T) calculations were performed with the MOLPRO 2002.3 program package.[44] Details of these calculations are reported in refs 37 and 38.

All the MRCI calculations were newly performed in the present work using the 2002.6 version of MOLPRO. Default parameters were generally used for the MOLPRO parameters, with the following exceptions: the SCF accuracy parameter was increased to 12, the energy convergence criterion for CAS and MRCI calculations was 1.0×10^{-10} E_h, and the PNORM parameter was set to 10^{-14} to obtain a smooth dissociation for eq 1.

2.1.1. CCSD(T). The low energy ab initio data of the PES used in the present work was described previously in ref 37. This surface has also been extended to cover a large region up to 20 000 cm^{-1} in a later work.[38] We have selected a subset of the CCSD(T) ab initio energies from ref 38, which are labeled CBS**.

This numerical PES is evaluated at the complete basis set (CBS) extrapolation level of theory using the fitting function $E = E_{CBS} + b/l^3$ where b is the fit parameter and l denotes the cardinal quantum number of the basis set series aug-cc-pV*l*Z (l = *T*,*Q*,5) from Dunning and co-workers.[45] This CBS PES was evaluated for a reduced set of points of the whole grid. The missing CBS points were generated by interpolation. The CBS** PES includes also the core−valence correlation energy contribution and relativistic corrections evaluated as the sum of the expectation values for the mass velocity and the one-electron Darwin terms. In the following, we will refer to these data with the simplified acronym CC.

2.1.2. MRCI. The low energy data described in section 2.1.1 are complemented with higher energy values obtained using an MRCI approach. These energies are calculated performing two independent MRCI calculations based on two-state CAS(8,7) wave functions in which excited configurations are limited to single and double excitations (MRCI(SD)) using the aug-cc-pVQZ basis[45,46] and including the Davidson correction.[47] The MRCI calculations employ the MOLPRO implementation of the internally contracted MRCI approach of Werner and co-workers.[48,49] The CAS space is a complete valence space where the 1s nitrogen orbital is kept doubly occupied and frozen. The (8,7) active space is the smallest possible CAS space that yields a balanced and physically meaningful description of the NH bond dissociation. In the following, we will refer to these data with the acronym MRCI.

The electronic ground state PES of ammonia contains peculiar features such as conical intersections with an excited state surface. A two-state CAS calculation is required in order to keep orthogonality and a well-behaved surface in the vicinity of these features.

Table 1 reports the MRCI dissociation energy (given here in terms of D_e, in units corresponding to wavenumbers) for different combinations of basis sets (*T*,*Q*), CAS reference states (1,2), and CAS active spaces (7,8,9,10). The dissociation energy hcD_e is evaluated as the difference between the MRCI energy obtained with the constraint of $r(NH_1)$ = 1000 pm and the fully optimized MRCI equilibrium energy for every combination separately. Both the raw D_e and the Davidson corrected D_e values are listed. We see that both values are most stable for the two-state CAS reference and the aug-cc-pVQZ basis set, which motivates our final choice of this combination; to limit the computational effort, we select an active space with 7 active orbitals.

In Table 1 we also give differences $(D_e - D_e^{(exp)})$, where $D_e^{(exp)}$ is an estimate of the dissociation energy of the reaction in eq 1 discussed below. These differences are roughly 1000 cm^{-1}, in the simultaneous two-state calculations after Davidson correction, which is related to the incomplete treatment of dynamic correlation in the MRCI(SD) calculation. As a comparison, in ref 31 the calculated dissociation energy is 4.4 eV (~35 500 hc cm^{-1}; 4.8 eV in ref 33), where the multiconfigurational quasidegenerate perturbation theory was used for the calculations.

At geometries close to the NH_3 equilibrium, the correlation energy recovered by CCSD(T) is 0.2718 E_h compared with only 0.2584 E_h for MRCI(SD). The difference amounts to approximately 13 mE_h (~3000 hc cm^{-1}) at equilibrium and decreases upon stretching of an NH bond, before the CCSD(T) approach starts to become inaccurate (beyond r(NH) ≈ 180 pm)

dx.doi.org/10.1021/jp4016728 | J. Phys. Chem. A 2013, 117, 7502−7522

Table 1. MRCI Dissociation Energies in Terms of Wavenumbers ($D_e = E_{diss}/hc$, in cm^{-1}) and Davidson Corrected Values[a]

basis l	CAS states	active orb.	D_e	$D_e - D_e^{(exp)}$	D_e (Davidson)	$D_e - D_e^{(exp)}$
T	1	7	39482.0	−1569.0	39017.9	−2033.1
T	1	8	41019.3	−31.7	40016.7	−1034.3
T	1	9	41128.8	77.8	39825.5	−1225.5
T	1	10	41451.9	400.9	39887.3	−1163.7
T	2	7	39444.1	−1606.9	40169.4	−881.6
T	2	8	40453.6	−597.4	39975.1	−1075.9
T	2	9	40949.8	−101.2	39857.5	−1193.5
T	2	10	41758.7	707.7	39844.1	−1206.9
Q	1	7	39887.4	−1163.6	39154.7	−1896.3
Q	1	8	41024.0	−27.0	40020.1	−1030.9
Q	1	9	40522.7	−528.3	39846.8	−1204.2
Q	1	10	40042.4	−1008.6	40017.9	−1033.1
Q	2	7	39271.3	−1779.7	40224.7	−826.3
Q	2	8	39809.4	−1241.6	39868.3	−1182.7
Q	2	9	39500.5	−1550.5	39879.2	−1171.8
Q	2	10	39551.0	−1500.0	39919.9	−1131.1

[a]Results are reported for two different basis sets (T = aug-cc-pVTZ, Q = aug-cc-pVQZ); MRCI calculations are performed using 1 or 2 CAS reference states and 4 different CAS spaces with 7, 8, 9, or 10 active orbitals. Errors are reported as differences $D_e - D_e^{(exp)}$, where $D_e^{(exp)} \approx 41\,051\ hc\ cm^{-1}$ is an estimation of the dissociation energy from thermochemical data (see text).

because of the multireference character of the system at large bond lengths.

For the calculation of a global PES, relative CCSD(T) data should be used in a region close to equilibrium, with the equilibrium energy or some energy close to that as reference energy, while relative MRCI data should be used at geometries far away from equilibrium, with a reference structure that is chosen such that size-consistency errors are expected to be minor. The merging of the two data sets is discussed in the following paragraph.

2.2. Merging. Within the merging strategy, we assume that the CCSD(T) points describe the region around the equilibrium structures well (both minima and the planar transition structure connecting them), whereas the MRCI data gives a correct, semiquantitative description of the asymptotic regions. Figure 2

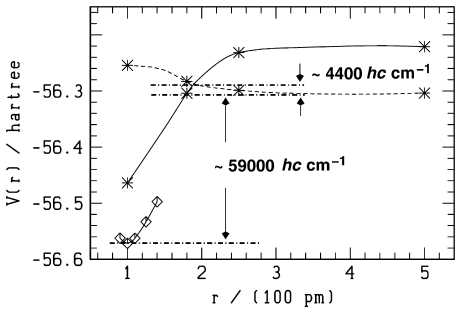

Figure 2. Electronic energies for planar ammonia as a function of one N−H distance r(N−H). Values for the remaining coordinates are: 100 pm (bond lengths), bond angles at 120°. The drawn lines are cubic spline interpolations and the different symbols correspond to (◊) CCSD(T) data from the present work; (*) MRCI data from the present work; (—) A_1 state in C_{2v}; (− −) B_1 state in C_{2v}.

indicates how values from these two data sets are related, by showing the energy of planar ammonia at varying values of one NH bond length. Because of the use of different basis sets and correlation treatments, the data are not comparable in absolute terms since the gap between the bottom of the CCSD(T) points and the MRCI points in the asymptotic region of channel 1 is on the order of 60 000 $hc\ cm^{-1}$, which does not even fall in the vicinity of the expected value for the dissociation energy.

In this article, we merge these different data sets into one single data set by a homogeneous shift of reference energies. Let $E_{ref}^{(CC)} = -56.5868\ E_h$ be the reference energy of the CCSD(T) data set; this is the lowest energy available in this data set at NH bond lengths of 101 pm and bond angles of 108° (CBS** value from ref 37, close to the equilibrium geometry). This energy is only 0.05 mE_h (11 cm^{-1}) above the minimum from the adjusted analytical representation of the PES in the present work.

The reference energy of the MRCI data set is chosen to be the lowest energy available in this data set under the constraint that one NH bond length is at least 1000 pm. Thus, the choice is made in this article to refer to the MRCI energy of the NH_2 product of reaction 1, rather than the NH_3 equilibrium energy. We obtain $E_{ref}^{(MRCI)} = -56.3123\ E_h$ at NH bond lengths of 102.2 pm and bond angle 102.8° of the residual NH_2 moiety, which is close to the optimized geometry. The energy difference $E_{ref}^{(MRCI)} - E_{ref}^{(CC)} = 0.2745\ E_h$ (60 246 $hc\ cm^{-1}$) is comparable to the gap from Figure 2 and much too high when compared to expected values of the dissociation energy.

An estimate of the dissociation energy for the reaction in eq 1 from thermochemical data[50] and an approximate harmonic zero point energy[22] yields $D_e^{(exp)} \approx 41\,051\ hc\ cm^{-1}$; anharmonic corrections will shift this value by about +50 to +100 $hc\ cm^{-1}$, roughly, which is a negligible error for the purposes of the merging procedure discussed in this section.

The MRCI and CC relative energies are then defined in the following way:

$$E_i^{(CC,rel)} = E_i^{(CC)} - E_{ref}^{(CC)} \quad (4)$$

$$E_i^{(MRCI,rel)} = E_i^{(MRCI)} - E_{ref}^{(MRCI)} + D_e^{(exp)} \quad (5)$$

The merged data set is the union of MRCI and CCSD(T) relative energies data sets:

$$\{E_i^{(CC,rel)}\} \cup \{E_i^{(MRCI,rel)}\}$$

This merging is quite smooth and, simultaneously, does account for the empirically determined dissociation energy. Sections of the analytical representation of the PES are shown below and underline the smoothness of this merging procedure. No exact data matching is required within the present adjustment strategy because the adjusted functional forms, which will be further described in section 2.4, are sufficiently stiff. Adjustments using more flexible forms such as high order polynomial forms could lead to strongly oscillating functions, when data matching is not exact.

A somewhat different merging strategy was used for the determination of a global PES for formaldehyde by Bowman and his co-workers.[25]

2.3. Variational Calculation of Vibrational Spectra. Vibrational spectra for the AMMPOT4 potential are calculated using a direct variational method based on an adiabatic contraction scheme.[51] The ro-vibrational Hamiltonian is formulated in terms of generalized internal coordinates following Meyer and Günthard.[52] As vibrational coordinates we chose the three NH bond lengths, the umbrella angle (the polar angle with respect to the molecular axis, see Figure 1) and two dihedral angles (rotation around the

dx.doi.org/10.1021/jp4016728 | J. Phys. Chem. A 2013, 117, 7502−7522

molecular axis of H-atoms 2 and 3 with respect to H atom 1). All ro-vibrational coupling tensor elements were calculated numerically on a grid in these coordinates. To solve the vibrational (i.e., $J = 0$) problem, we employed a generalized discrete variable representation (DVR) in the six vibrational coordinates.[51] With the exception of the dihedral angles, grids were further contracted by using the near-variational potential-optimized DVR approach of Wei[53] (see also ref 54). The final grids consisted of $8^3 \times 51^2 \times 25$ points for eigenstates up to $v_{NH} = 3$. The vibrational Hamiltonian was diagonalized using the successive truncation−diagonalization procedure described in ref 51, systematically checking the convergence of eigenvalues to at least 0.1 cm^{-1} (tunnelling splittings to within 0.01 cm^{-1}) with respect to the coordinate grid and all truncation parameters. Transition moments were calculated using previously published dipole moment functions[40,55] defined in an instantaneous Eckart system with respect to C_{3v} reference geometries (i.e., displacement in coordinates with E-symmetry set to zero). The transformation to the Eckart system was effected using the method of ref 56. The ro-vibrational Hamiltonian was diagonalized in a direct product basis of vibrational eigenfunctions and rigid symmetric rotor eigenfunctions.

For a quick evaluation of vibrational transitions, we have also used the MULTIMODE program.[57] This program has also been employed in the past to calculate the vibrational spectrum of ammonia, but the calculation did not converge for many transitions because of basis set limitations, the approximations inherent to this method, or both.[41] However, some transitions could be calculated quite reliably, when compared to a direct variational method. Here, we found that all totally symmetric transitions of NH_3 up to 4000 cm^{-1}, fundamental and overtones, as well as the tunneling doublets thereof, could be converged, when compared to the direct variational method. There are 13 of these (which are marked in Table 6 below).

We also present here data from a new evaluation of the YZLJT PES[38] using the TROVE program.[58] This is a variational program designed to calculate the rotation-vibration energies of an arbitrary polyatomic molecule in an isolated electronic state. A basic feature of this program is the use of expansions in linearized vibrational coordinates to represent both the kinetic energy operator and the potential energy function. Presently the expansions of the kinetic energy and potential energy operators are truncated after the sixth and eighth order terms, respectively. For NH_3, we use the HBJ nonrigid-reference configuration method by Hougen et al.[59] with the umbrella coordinate representing the nonrigid large amplitude motion. The present choice of the coordinates is consistent with ref 38. Our basis set is constructed from one-dimensional functions obtained by numerically solving the corresponding one-dimensional Schrödinger Equation problems by means of the Numerov−Cooley method.[58,60] In TROVE calculations, the size of the vibrational basis set is controlled by the polyad number P defined in ref 38. In the construction of the rovibrational Hamiltonian matrix, we include vibrational basis functions with $P \leq P_{max}$. For the YZLJT PES,[38] we computed five sets of vibrational energies for $P_{max} = 10$, 12, 14, 16, and 18, which were then extrapolated to the complete vibrational basis set (CVBS) limit.[61] The resulting CVBS term values are collected in Tables 6−9.

2.4. Analytical Potential and Adjustment Procedure. The analytical, six-dimensional function used to represent the PES is described in ref 22. The parameter values are given in Table 4. They were obtained from a series of adjustments of the analytical representation to the combined set of ab initio data described in section 2.2 and define the representation called AMMPOT4. For the adjustments, a modified version of the Levenberg−Marquardt algorithm[62] was used that allows us to satisfy analytical relations between parameters during the adjustment loops, with the help of Lagrange multipliers, as described in previous work.[7,22] We do not consider minimization of the resulting root-mean-square deviation as the ultimate optimization criterion. Rather, the optimal parameter set has to satisfy additional, nonanalytical conditions from further graphical and numerical analysis of the representation. Numerical analysis includes the calculation of characteristic features of the PES, such as the geometries, energies, gradients, and second derivatives at stationary points, and the variational calculation of vibrational spectra. In the graphical analysis, we compare several one- and two-dimensional sections of the PES representation with the ab initio data, to ensure its qualitatively correct behavior. In the following, the adjustment procedure adopted in this work is described in more detail.

2.4.1. Asymptotic Limits. Similarly to the procedure adopted in ref 22, we first adjusted parameters that describe the asymptotic limits to separate data sets obtained by evaluation of published analytical PES representations of NH_2,[63] NH,[64] and H_2.[65] The adjustment is done considering additional conditions related to the harmonic force field, dissociation energies, and further energies such as the barrier to linearity in NH_2, as in ref 22. For NH_2 (second column in Table 4), a set of parameter values was obtained here that is somewhat different from that defining the AMMPOT2 representation.[22] AMMPOT2 and AMMPOT4 are essentially equivalent representations of the same PES, in the asymptotic limits NH_2 and NH (parameter a_r has no influence in the NH limit).

2.4.2. Raw Adjustment Steps. In a first series of adjustment steps, a raw set of adjusted values is searched by allowing all parameters in Table 4 to vary, with the exception of the equilibrium bond lengths and angles and of those parameters whose values are effectively an integer. The latter are varied manually, and an optimal choice is made upon graphical analysis. Equilibrium bond lengths and angles were initially chosen to coincide with the values given in ref 37, i.e., $r_e = 101.03$ pm and $\alpha_e = 106.75°$, but were allowed to change in the subsequent fine adjustment steps discussed below. In the raw adjustment steps, the Marquardt algorithm was run with parameter $\lambda = 100$.

In the present work, fourth order anharmonic parameters in the bending potential are varied, in contrast to AMMPOT2, where these parameters were fixed to zero. We found that a variation of these parameters is necessary to obtain a qualitatively correct description of the potential energy surface in regions of configuration space that surround the S_0-T_1 intersystem crossing seams. However, from the graphical analysis of sections along reaction channel of eq 3, we found that the present, limited set of ab initio data is insufficient to allow for a numerically converged determination of these parameters. We therefore determined them from stepwise, manual variations and inspection of graphical outputs at each step.

2.4.3. Fine Adjustment Steps. In the second series of adjustment steps, a reduced set of parameters was varied, starting from the raw values obtained in the preceding step, with parameter $\lambda = 2$ in the Marquardt algorithm, allowing us thus to stay closer to the quadratically converged limit of this algorithm. We varied all parameters directly related to the harmonic force constants and anharmonicity parameters. For the bending potentials, only anharmonicity parameters up to the third order were varied. All other parameters, including the pair potential parameter $D_P^{(I)}$ and damping parameters (see ref 22), were kept fixed.

dx.doi.org/10.1021/jp4016728 | J. Phys. Chem. A 2013, 117, 7502−7522

In all fine adjustment steps, eight additional conditions are considered among the parameters. Six conditions correspond to the six harmonic force constants, and one condition is related to the dissociation energy of channel of eq 1 (see discussion of the value $D_e^{(exp)} \approx 41\,051\ hc\ cm^{-1}$ above). One final condition imposes a potential value close to 1788 $hc\ cm^{-1}$ for a planar NH_3 structure with equal bond lengths of 99.4 pm. These values agree well with results from accurate theoretical treatments of the inversion barrier in ammonia.[63,66,67]

The harmonic force constants were chosen to coincide with values calculated from a finite difference evaluation of the PES from ref 14. This set of constraints should allow us to guide the adjustment toward a closer agreement with experimental data. In our previous work on the global potential energy surface of methane,[7] this strategy was adopted successfully using an equilibrium geometry and a harmonic force field that were derived from experimental data.[68] In the case of ammonia, however, no equivalent determination of an experimental equilibrium structure and harmonic force field exists. We therefore use results from the PES developed in ref 14 since that PES provides vibrational energy levels agreeing well with experiment at low energies.

In each one of final adjustment steps, a vibrational spectrum was calculated with MULTIMODE and the 13 totally symmetric transitions of NH_3 up to 4000 cm^{-1}, that are defined in section 2.3 and in Table 6a, were compared to their experimental values. In some cases, vibrational states were also calculated directly. Each step allowed us to improve the agreement with experimental values. The following actions were taken.

(1) Scaling of equilibrium constants. Following an idea used in ref 11, equilibrium geometry parameters are scaled by factors S_r and S_α, which are obtained from the ratio of experimentally available values of equilibrium constants to theoretically determined, vibrationally averaged values. Theoretical values for vibrationally averaged equilibrium constants r_0 and α_0 were determined from ro-vibrational transitions $\tilde{\nu}_{v=0,J,K}$, which were calculated with our direct variational method on the PES resulting from the raw adjustment step in section 2.4.2. From evaluations of the approximate relations

$$\tilde{\nu}_{v=0,J,K} \approx \tilde{\nu}_0 + B_0 J(J+1) + (C_0 - B_0)K^2 \tag{6}$$

for $J = 0,1$ and $K = 0,1$, we obtained $B_0 \approx 9.971\ cm^{-1}$ and $C_0 \approx 6.240\ cm^{-1}$ in the lower component of the ground state tunneling doublet. By interpreting $B_0 = h/8\pi^2 cI_B$ and $C_0 = h/8\pi^2 cI_C$ and using analytical relations between the main moments of inertia I_B and I_C and internal coordinates, one derives the following formulae:

$$r_0 = \frac{h}{2\pi \sin(\chi_0)} \frac{1}{\sqrt{6cm_H C_0}} \tag{7}$$

$$\alpha_0 = \arccos\left(\frac{3}{2}\frac{1}{\cos^2(\chi_0)} - \frac{1}{2}\right) \tag{8}$$

where

$$\chi_0 = \frac{1}{2}\arccos\left(\frac{3(B_0/C_0)(m_H + m_N) - 6m_H - 2m_N}{(B_0/C_0)(3m_H - m_N) - 6m_H - 2m_N}\right). \tag{9}$$

With $m_H = 1.007825$ Da and $m_N = 14.00307$ Da, we obtain $\alpha_0^{(the)} \approx 107.52°$ and $r_0^{(the)} \approx 101.5$ pm, which we compare to $\alpha_0^{(exp)} \approx 107.8° \pm 0.1°$ and $r_0^{(exp)} \approx (101.73 \pm 0.2)$ pm.[69] This yields $S_r = r_0^{(exp)}/r_0^{(the)} \approx 1.0023$, and $S_\alpha = \alpha_0^{(exp)}/\alpha_0^{(the)} \approx 1.0026$. Consequently, we scale the equilibrium geometry parameters as follows:[14]

$$r_e = S_r r_e^{(raw)} = 101.26\ pm \approx 101.28\ pm \tag{10}$$

$$\alpha_e = S_\alpha \alpha_e^{(raw)} = 107.03° \tag{11}$$

While the scaled value for r_e is very close to the value of 101.28 pm given in ref 14, the scaled value for the equilibrium bond angle α_e is about 0.5° larger than the value given in that work. For r_e, we adopt here the value given in ref 14; for α_e, we use the value given in eq 11. These values agree well with the equilibrium structure of ammonia as estimated in ref 70 from an evaluation of experimental rotational constants and rotation−vibration interaction constants from high level ab initio theory.

(2) Scaling of harmonic and anharmonic parameters related to the ν_4 mode. In preliminary adjustment steps, we found that, among the 13 totally symmetric levels studied, the first overtone $4^{2,0}$ of the doublet of the degenerate bending mode ν_4 around 3215 cm^{-1} turned out to be too high by about 30 cm^{-1}, when compared to the experimental values. In order to remedy this, we have scaled down the f_{b_2} parameter by a ratio that corresponds to the square of 3215/(3215 + 30). This ratio was also used to scale down the F_{34} and F_{44} harmonic force constants, correspondingly. Additionally, parameter $a_{b_2}^{(S2)}$ was scaled up by the factor 1.1. These two parameters were then fixed at the resulting values, which are given in Table 4, in the final fine adjustment steps.

(3) Scaling of the harmonic force constant related to the ν_1 mode. In other preliminary adjustment steps, we also found that, after the changes made in the preceding step, the totally symmetric stretching mode ν_1 decreases by 20 cm^{-1}, roughly. In order to remedy this, we scaled down the harmonic force constant F_{11} by a factor that corresponds to the square of (3335 − 20)/3335 (3335 cm^{-1} is approximately the experimental value of the ν_1 fundamental). In the final step, we adjusted a reduced set of parameters with only three constraints, namely, on F_{11}, F_{33}, and F_{34}. The resulting set of parameters is given in Table 4.

2.5. Symmetry and Notation. While the equilibrium geometry of ammonia (Figure 1) corresponds to the point group C_{3v}, it is the prototypical nonrigid molecule due to the low barrier to inversion. The group suitable for classifying the symmetry of vibrational and ro-vibrational levels following Longuet Higgings[71] is then the molecular symmetry group $\mathbf{M}_{s12} = \mathbf{S}_3^* = \mathbf{S}_3 \otimes \mathbf{S}^*$ of the permutation of the three protons ($\mathbf{S}_3$) and inversion ($\mathbf{S}^*$), isomorphous to D_{3h}. The inversion sublevel structure can be obtained from the induced representation $\Gamma_m \uparrow \mathbf{S}_3^*$, where Γ_m is the symmetry in the subgroup $\mathbf{M}_{s6}$ of $\mathbf{M}_{s12}$, which is isomorphous to C_{3v}. For convenience, we give in Tables 2 and 3 the corresponding character tables that also define the notation.

Table 2. Character Table of the Subgroup $\mathbf{M}_{s6}$ of the Molecular Symmetry Group $\mathbf{M}_{s12}$ (= $\mathbf{S}_3^*$), and Induced Representations $\Gamma_m \uparrow \mathbf{S}_3^*$. $\mathbf{M}_{s6}$ is Isomorphous to the Point Group C_{3v}

Γ	E	$2C_3$	$3\sigma_v$	
$\mathbf{M}_{s6}$	E	2(123)	3(12)*	$\Gamma(\mathbf{M}_{s6}) \uparrow \mathbf{S}_3^*$
A_1	1	1	1	$A_1^+ \oplus A_2^-$
A_2	1	1	−1	$A_2^+ \oplus A_1^-$
E	2	−1	0	$E^+ \oplus E^-$

We note that this notation gives parity (positive or negative) as an upper index, and the symbols A_1, A_2, and E define the species

dx.doi.org/10.1021/jp4016728 | J. Phys. Chem. A 2013, 117, 7502−7522

Table 3. Character Table of the Molecular Symmetry Group $\mathbf{M}_{s12}$, Isomorphous to the Point Group D_{3h}

Γ	Γ	E	$2C_3$	$3C_2'$	σ_h	$2S_3$	$3\sigma_v$
$\mathbf{M}_{s12}$	D_{3h} (M)	E	2(123)	3(12)	E^*	2(123)*	3(12)*
A_1^+	A_1'	1	1	1	1	1	1
A_2^+	A_2'	1	1	−1	1	1	−1
E^+	E'	2	−1	0	2	−1	0
A_1^-	A_1''	1	1	1	−1	−1	−1
A_2^-	A_2''	1	1	−1	−1	−1	1
E^-	E''	2	−1	0	−2	1	0

in the permutation group $\mathbf{S}_3$ (see refs 72 and 73). Similarly for NH_2D and NHD_2, one has the relevant group $\mathbf{M}_{s4} = \mathbf{S}_2^* = \mathbf{S}_2 \otimes \mathbf{S}^*$, where the permutations concern protons for NH_2D and deuterons for NHD_2.

3. RESULTS

3.1. Fits. The fit was performed on a selected choice of roughly 10 000 points from ref 38, and 500 points from MRCI calculations from the present work. The selection was made on the basis of a coarse grained distribution of geometries.

Table 4 collects the resulting parameter values for the fit in column "NH_3". The values listed under columns "NH_2" and "NH" are from new adjustments of the PES of those molecules as described before.

The quality of the fit will be judged from graphical analyses and from the calculation of vibrational spectroscopic data below. It might nevertheless be useful to give the following statistics of the present adjustment: the averaged absolute differences between the final fit and the underlying ab initio points is 100 cm^{-1} for points below 3000 cm^{-1} (1150 points), 200 cm^{-1} for points between 3000 and 6000 cm^{-1} (2450 points), 450 cm^{-1} for points between 6000 and 10 000 cm^{-1} (2000 points), 850 cm^{-1} for points between 10 000 and 15 000 cm^{-1} (1800 points), 1150 cm^{-1} for points between 15 000 and 20 000 cm^{-1} (2000 points), 1500 cm^{-1} for points between 20 000 and 25 000 cm^{-1} (400 points), and 1000 cm^{-1} for points above 25 000 cm^{-1} (600 points). As a test, a similar distribution of errors is obtained if differences are calculated with respect to the complete data set of more than 51 000 points from ref 38.

We note that most parameters in the "stretch" and "pair" parts of the representation have values quite similar to those of AMMPOT2 (apart from a_r and D_{ij}^0). However, parameters belonging to the "bend" part of the representation have changed considerably since terms of up to order 4 have been included in the representation of AMMPOT4, while the maximum order was 3 in AMMPOT2.

We note also that some of the damping parameters have been varied under constraints (see footnote b of Table 4). A total of 25 parameters that describe the NH_3 moiety have been varied automatically during the adjustment procedure; these are parameters having 7 to 8 nonzero digits after the period in column NH_3, which had to satisfy eight additional conditions, leading to a net number of 17 freely adjusted parameters. More parameters that appear with zeros in the fifth to eight digit after the period were varied manually. Even if all parameters are needed to complete the analytical representation, their total number is much smaller than the number of parameters used in previous analytical representations of the PES of ammonia, as discussed in ref 22.

3.2. Topography of the PES and Ammonia Thermochemistry. *3.2.1. Dissociation Channel of eq 1.* Figure 3 shows one-dimensional sections of the PES along one N−H distance. The two different types of marks indicate the two different sets of ab initio data used for the fit. Their position relative one to the other was determined as described before in section 2.2. The CCSD(T) data (marked with ◇) are restricted to variations of the N−H distance of ±50 pm around the equilibrium distance of 101.28 pm and to energies up to 15 000 hc cm^{-1}, roughly. The figure gives the impression that the number of points from CCSD(T) used in the fit is smaller than the number of MRCI points (marked with *); in fact, the number of CCSD(T) points exceeds that of the MRCI data by a factor of 20, as mentioned above. Because of the scale of the figure, individual adjustment errors are not recognizable in the lower energy range. The continuous line is an evaluation of the current AMMPOT4 PES; the broken line refers to AMMPOT2 from ref 22. Both lines agree well on the scale of the figure, the formation of the barrier at the conical intersection being somewhat less pronounced for AMMPOT4. Clearly both representations are qualitatively quite similar. The optimized dissociation energy, after relaxation of the NH bond lengths and bond angle in the NH_2 product, is 41 051 hc cm^{-1} and equals the experimental estimate we give, in this article, by construction (see Table 5).

The occurrence of a barrier replacing the conical intersection in the one-dimensional section of Figure 3b is a direct consequence of the single-valued analytical representation. The molecular structure does not correspond to a stationary point of the potential at this position, when all degrees of freedom are considered. The conical intersection seam in ammonia is four-dimensional, and the PES varies along this seam. For instance, the position of the conical intersection varies from $r(NH) \approx 210$ pm to $r(NH) = \infty$, when the remaining bond angle varies from $\alpha = 120°$ to $\alpha = 180°$; the energy at $r(NH) \to \infty$ and linear NH_2 is given by $D_e^{(exp)} + E_{NH_2}^{(lin)} \approx (41\,051 + 11\,900)\ hc\ cm^{-1} = 52\,951\ hc\ cm^{-1}$, relative to the NH_3 equilibrium, where $E_{NH_2}^{(lin)} \approx 11\,900\ hc\ cm^{-1}$ is the barrier to linearity of NH_2.[22]

The energy at the conical intersection indicated in Figure 2 is expected to be close to the lowest energy of the corresponding conical intersection seam, which has not yet been fully determined.[30,31] This energy is roughly 4400 hc cm^{-1} above the dissociation limit of eq 1 (equivalent to 20 mE_h). The corresponding barrier energy of AMMPOT4, in Figure 3b, is around 800 hc cm^{-1}. This allows us to make the following, rather conservative estimation: the present PES should be useful in reactive scattering calculations involving the recombination reaction

$$NH_2(^2B_1) + H(^2S_{(1/2)}) \rightarrow NH_3(^1A_1) \qquad (12)$$

at total collision energies of less than 800 hc cm^{-1}, i.e., at collision temperatures of less than 400 K, typically.

3.2.2. Potential at Large Angular Displacements. Figure 4 shows one-dimensional sections of the PES along the inversion angle χ (see Figure 1). Here, too, one sees that both PES representations follow but do not coincide exactly with the ab initio data, at higher energies, while they almost overlap at lower energies. We expect that the true representation of the PES of ammonia will lie nearby both representations. This figure thus also allows us to estimate an error of $\pm 1000 - 2000$ cm^{-1} that can be expected for evaluations of our representation at single points in the region above 15 000 cm^{-1}.

The error is significantly smaller in the low energy region. Figure 5 supports this finding and indicates that, in the asymptotic region of the reaction channel of eq 1, the PES is a faithful representation of the ab initio data.

dx.doi.org/10.1021/jp4016728 | J. Phys. Chem. A 2013, 117, 7502−7522

Table 4. Parameters Used to Define the Present Global Analytical Representation of NH_3 to NH. 1 Å = 100 pm

	NH_3	NH_2	NH
$V_{stretch}$ Parameters			
$a_r/(Å^{-1})$	2.2101896	3.0655330	3.0655330
$r_e/(Å)$	1.0128000	1.0260000	1.0363500
$f_s/(aJ\ Å^{-2})$	6.4220980	6.2874970	6.3928490
$a_s/(Å^{-1})$	2.1520016	2.2486020	2.1560860
ε_6	0.0844658	0.0683101	0.0023672
ε_8	0.0000000	0.0000000	−0.1100000
$r_s/(Å)$	2.0000000	2.0000000	2.1500000
V_{pair} Parameters			
$D_{ij}^0/(aJ)$	1.0809020	1.0000000	*a*
$a_{ij}^0/(Å^{-1})$	0.4766339	0.5064664	
$r_{ij}^\infty/(Å)$	0.7414000	0.7414000	
$a_{ij}^\infty/(Å^{-1})$	1.9453400	1.9453400	
$D_{ij}^\infty/(aJ)$	0.7605968	0.7605968	
V_{bend} Parameters			
$a_c/(Å^{-1})$	1.4720143	1.4720143	*a*
c_e	−0.2928836	−0.2368381	
$f_{b_1}/(aJ)$	0.0588056	0.1377804	
$f_{b_2}/(aJ)$	0.1288000	0.1000000	
$a_{b_{2_1}}^{(S1)}$	−0.3238790	−0.3784674	
$a_{b_{2_2}}^{(S1)}$	1.6025190	−0.3784674	
$a_{b_{3_1}}^{(S1)}$	0.1575220	−0.0948867	
$a_{b_{3_2}}^{(S1)}$	3.6579140	−0.0948867	
$a_{b_{3_3}}^{(S1)}$	0.9482045	−0.0948867	
$a_{b_{4_1}}^{(S1)}$	0.0110993	0.0000000	
$a_{b_{4_2}}^{(S1)}$	−3.8190330	0.0000000	
$a_{b_{4_3}}^{(S1)}$	−2.2165740	0.0000000	
$a_{b_{4_4}}^{(S1)}$	−2.4830280	0.0000000	
$a_{b_{2_1}}^{(S2)}$	−1.6000000	0.0000000	
$a_{b_{2_2}}^{(S2)}$	−0.8000000	0.0000000	
$a_{b_{3_1}}^{(S2)}$	−2.2000000	0.0000000	
$a_{b_{3_2}}^{(S2)}$	−2.0000000	0.0000000	
$a_{b_{3_3}}^{(S2)}$	0.0280000	0.0000000	
$a_{b_{4_1}}^{(S2)}$	3.1000000	0.0000000	
$a_{b_{4_2}}^{(S2)}$	4.6000000	0.0000000	
$a_{b_{4_3}}^{(S2)}$	2.5000000	0.0000000	
$a_{b_{4_4}}^{(S2)}$	0.0800000	0.0000000	
$a_{b_{4_5}}^{(S2)}$	0.1300000	0.0000000	
Damping Parameters[b]			
$a_{d_{xc}}^{(a1)}$	1.5139000	1.0000000	*a*
$a_{d_{xc}}^{(a3)}$	1.0000000	1.0000000	
$a_{d_{xo}}^{(a1)}$	1.4048880	1.0000000	
$a_{d_{xo}}^{(a3)}$	1.0000000	1.0000000	
$a_{d_{lc}}^{(a1)}$	0.0000000	0.0000000	
$a_{d_{lc}}^{(a3)}$	0.0000000	0.0000000	
$a_{d_{lo}}^{(a1)}$	−1.0000000	−1.0000000	
$a_{d_{lo}}^{(a3)}$	−1.0000000	−1.0000000	
$a_{d_{xc}}^{(e1)}$	2.1361563	1.0000000	
$a_{d_{xc}}^{(e3)}$	1.0000000	1.0000000	
$a_{d_{xo}}^{(e1)}$	−0.2057619	1.0000000	
$a_{d_{xo}}^{(e3)}$	1.0000000	1.0000000	
$a_{d_{lc}}^{(e1)}$	0.0000000	0.0000000	
$a_{d_{lc}}^{(e3)}$	0.0000000	0.0000000	
$a_{d_{lo}}^{(e1)}$	−1.0000000	−1.0000000	
$a_{d_{lo}}^{(e3)}$	−1.0000000	−1.0000000	
$a_{d_{xc}}^{P}$	0.8030900	1.0000000	
$a_{d_{xo}}^{P}$	1.1126840	1.0000000	
$a_{d_{lc}}^{P}$	0.0000000	0.0000000	
$a_{d_{lo}}^{P}$	−0.5000000	−1.0000000	
n_{d_l}	1.0000000	1.0000000	
n_{d_x}	2.0000000	2.0000000	
$n_{d_{cos}}$	1.0000000	1.0000000	
Switching Parameters			
n_{sb}	6.0000000	6.0000000	6.0000000
$r_{sb}/(Å)$	2.0000000	2.0000000	2.0000000
n_{db}	6.0000000	6.0000000	
$r_{db}/(Å)$	2.0000000	2.0000000	

[a]Empty cells are parameters that were either found to be effectively irrelevant for the fit or cannot be defined within certain subsets; where appropriate, the value 0.0 can be set. [b]The superindex *p* on $a_{d\alpha}$ parameters ($\alpha = x$ or *l*) indicates parameters used in V_{pair} and superindices (a*n*) or (e*n*) indicate parameters used in a- and e-type expressions of power *n* in V_{bend}, respectively. During the fit, parameters were adjusted under the constraints $a_{d_{x\beta}}^{(a2)} = a_{d_{x\beta}}^{(a1)}$, $a_{d_{l\beta}}^{(a4)} = a_{d_{l\beta}}^{(a3)}$, $a_{d_{x\beta}}^{(e2)} = a_{d_{x\beta}}^{(e1)}$, and $a_{d_{l\beta}}^{(e4)} = a_{d_{l\beta}}^{(e3)}$ (α = x or l; β = c or o).

For a comparison between different analytical representations of the PES of ammonia along this and other sections of coordinate space, we refer to ref 22, where acronyms were introduced. The potentials proposed by Huang, Schwenke, and Lee (HSL-0 PES[36] and HSL-2 PES[16]) are polynomial expansions over a large number of terms. For the HSL-0 PES, 3393 parameters were adjusted to about 8000 high level ab initio energy points including both the coupled cluster and coupled pair approaches. Its form is somewhat similar to the LTYCJ/YZLJT PES,[37,38] and it was clearly designed to well reproduce the ro-vibrational spectrum of ammonia, as will be discussed below. Despite its global attribute, at present, it is not clear whether the HSL-0 and HSL-2 PES are really global. Indeed, in ref 36, the dissociation energy was set to 50 520 *hc* cm^{-1}, which is 25% higher than the value estimated above for $D_e^{(exp)}$. This indicates that the HSL-0 PES is probably correlated asymptotically with the $^2A_1$ channel of eq 2, as is the LTYCJ PES (see ref 22).

3.2.3. Dissociation Channel of eq 3. For the rupture of two NH bonds, AMMPOT4 represents first the singlet state and then, beyond the region of the intersystem crossing, the lower lying triplet state points. Such a PES may be called post-spin-orbit (SO) adiabatized.

dx.doi.org/10.1021/jp4016728 | J. Phys. Chem. A 2013, 117, 7502−7522

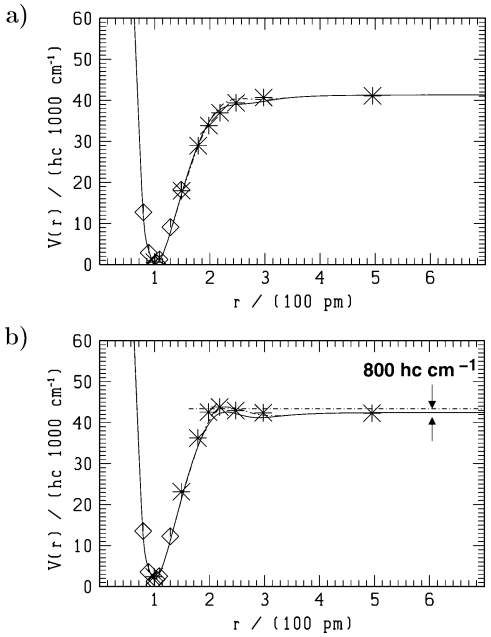

Figure 3. One dimensional sections of the potential energy surface of ammonia as a function of one N−H distance r(N−H). (a) Pyramidal ammonia. Values for the remaining coordinates are bond lengths at 101.2 pm and bond angles at 106.5°; this is almost the equilibrium bond angle. The inversion angle out of the planar structure is $\chi = 112.3°$. (b) Planar ammonia. Bond lengths are roughly 101.2 pm, bond angles at 120°, and inversion angle $\chi = 90°$. The different symbols correspond to (◊) CCSD(T) data from the present work; (*) MRCI data from the present work; the combination of both data sets into a single set of ab initio data is discussed in section 2.2; (—) present work (AMMPOT4); (– –) from ref 22 (AMMPOT2).

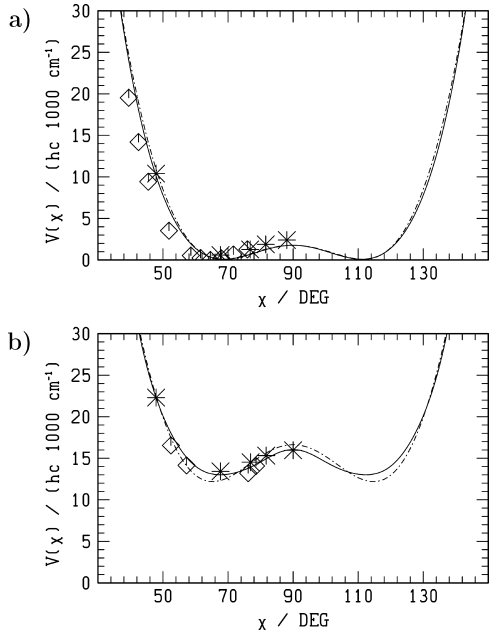

Figure 4. One dimensional sections of the potential energy surface of ammonia as a function of the inversion angle χ (see Figure 1). (a) Bond lengths are at 101.2 pm, bond angles change upon conservation of C_{3v} symmetry (regular pyramids). (b) As in panel a, but bond angles change upon conservation of C_s symmetry (planar ammonia forms a "T" and pyramids are distorted). See also text and Figure 3 for a description of symbols.

Post-SO-adiabatic potential energy curves have been used in the description of the photodissociation of trimethyltiniodide.[74]

AMMPOT4 was obtained by an additional, manual adjustment of certain parameters such that the PES follows more closely the triplet state beyond the intersystem crossing. The reason for this ad hoc procedure is that the set of previously calculated triplet CASPT2 points[22] is sparse and has not allowed for a systematic adjustment of all parameters. As a consequence, the representation is only of qualitative character and must be considered preliminary, in this region of configuration space. An improvement of the description is foreseen, in future work, by inclusion of ab initio data obtained at the MRCI level for spin−orbit couplings, and a systematic and automatic adjustment within a procedure as described before in section 3.1. It will be important to give more flexibility to damping and switching parameters.

Figure 6 shows a two-dimensional section of AMMPOT4 along the coordinate R and the coordinate d, which gives the interatomic distance in the departing H_2 moiety, indicating the complexity of the potential energy landscape predicted for the reaction channel of eq 3. The figure suggests the existence of several saddle points in that region. A systematic search in the six-dimensional coordinate space yields one second order saddle point at $E \approx 38\,400\ hc\ \mathrm{cm}^{-1}$ and coordinates $r_1 = 1.0398$ Å, $r_2 = r_3 = 2.1392$ Å and $\alpha_{12} = \alpha_{13} = 75.32°$, $\alpha_{23} = 20.93°$. Further information on saddle points and other characteristic points of the present PES are collected in Table 5.

The saddle point at roughly 38 400 cm^{-1} is of C_s symmetry and is located close to the saddle at $R \approx 220$ pm and $d \approx 70$ pm in the two-dimensional surface shown in Figure 6. It links the NH_3 equilibrium structure and the almost isoenergetic outgoing reaction channel asymptote of eq 3. The dissociation energy along this channel is 38 484 $hc\ \mathrm{cm}^{-1}$.

Considering the variation of zero-point energy in the harmonic approximation, given in Table 5, we obtain, for the reaction of

Table 5. Collection of Key Data Regarding the Topography of the Present, Global PES for the Electronic Ground State of Ammonia (NH_3): Geometries, Energies, and Gradients of Stationary Points[a]

	r_i/(Å)/α_{ij}/(deg)	$E/(hc\ \mathrm{cm}^{-1})$	$E_{zp}/(hc\ \mathrm{cm}^{-1})$	$(\partial^2 E/\partial Q_j^2)^{1/2}/(c\ \mathrm{cm}^{-1})$[b]					
C_{3v}	1.0128(3)/ 107.03(3)	0	7500[c]	3608	3607	3452	1652	1651	1030
D_{3h}	0.9988(3)/ 120.00(3)	1774	7301[c]	3800	3799	3536	1734	1734	855*i*
C_s[d]	1.04, 2.14(2)/ 75.2, 75.2, 20.9	38357	4772[c]	4172	3373	1341	657	1118*i*	1251*i*
C_{2v}[e]	1.026(2)/ 103.7(1)	41051	4223[c]	3504	3386	1557			
$C_{\infty v}$[f]	1.03635(1)/0.7414(1)	38484	3896[c,h]	3397	4395[g]				

[a]Geometries are given in terms of the internal coordinates defined in Figure 1. The values in parentheses give the number of identical coordinate values. [b]Normal coordinates defined with respect to the stationary point; negative second derivatives have imaginary units; masses m(H) = 1.007 25 u and m(N) = 14.0 u. [c]Harmonic zero-point energy obtained from the sum over all real frequencies. [d]Saddle point for NH_3 ($^3A_1$) → NH ($^3\Sigma^-$) + H_2 ($^1\Sigma_g^+$). [e]NH_2 ($^2B_1$) + H ($^2S_{(1/2)}$) (asymptote, eq 1). [f]NH($^3\Sigma^-$) + H_2 ($^1\Sigma_g^+$) (asymptote, eq 3). [g]H_2 harmonic frequency from ref 65. [h]Sum of NH and H_2 harmonic zero-point frequencies.

dx.doi.org/10.1021/jp4016728 | J. Phys. Chem. A 2013, 117, 7502−7522

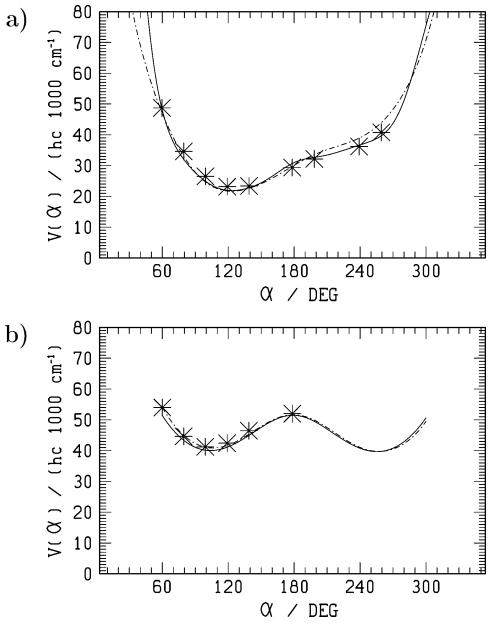

Figure 5. One dimensional sections of the potential energy surface of planar ammonia as a function of the bond angle $\alpha_{23} = \alpha$ (see also Figure 1). Bond lengths are such that $r_2 = r_3 = 100$ pm and bond angles are $\alpha_{12} = \alpha_{13} = (180° - \alpha)/2$. Bond length (a) $r_1 = 150$ pm and (b) $r_1 = 300$ pm. See also text and Figure 3, where further symbols are defined.

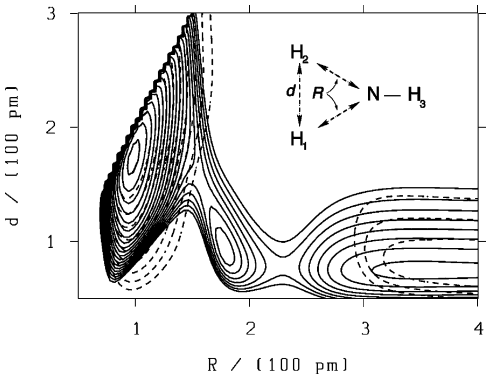

Figure 6. Two-dimensional section of the potential energy surface (AMMPOT4) of planar ammonia as a function of the coordinates R and d (see the insert for a proper definition); the remaining coordinates are such that $r_3 = 100$ pm, all atoms are within the same plane (planar ammonia structure), and C_{2v} symmetry is maintained. The different contour line types correspond to (—) present work (AMMPOT4) and (– –) from ref 22(AMMPOT2). Contour lines link isoenergetic points, and the separation between them is 3000 (AMMPOT4) and 6000 cm^{-1} (AMMPOT2); the smallest shown contour line is around the point $R \approx$ 100 pm and $d \approx$ 170 pm and corresponds to 3000 cm^{-1} for both potentials; the largest shown contour line is at 60 000 cm^{-1} for AMMPOT4 and 57 000 cm^{-1} for AMMPOT2; barriers for AMMPOT4 at about $R \approx$ 220 and 160 pm correspond to roughly 55 000 cm^{-1} and 46 000 cm^{-1}, respectively.

eq 13, a zero Kelvin reaction enthalpy $\Delta_{13}H_0^{\ominus} \approx -417$ kJ mol^{-1} for AMMPOT4, which is within acceptable thermochemical accuracy when compared to the experimental value $\Delta_{13}H_0^{\ominus} \approx -414$ kJ mol^{-1} from ref 75.

The effective barrier for the (spin forbidden) insertion of molecular hydrogen in triplet imidogen

$$NH(^3\Sigma^-) + H_2(^1\Sigma_g^+) \rightarrow NH_3(^1A_1) \quad (13)$$

is estimated be on the order of 9 kJ mol^{-1} (equivalent to 750 cm^{-1}), if the variation of zero-point energy is taken into account in the harmonic approximation (see Table 5). A different saddle point is expected to exist for the abstraction reaction

$$NH_2(^2B_1) + H(^2S_{(1/2)}) \rightarrow NH(^3\Sigma^-) + H_2(^1\Sigma_g^+) \quad (14)$$

In ref 76, a barrier of 38 kJ mol^{-1} was computed for this reaction at a correlation energy scaled Moller–Plesset theoretical level; however, neither triplet states nor spin–orbit coupling have been considered explicitly in ref 76. On the AMMPOT4 PES, this reaction should be almost barrierless. This point needs to be verified in future work, after additional calculations on the lowest triplet state of ammonia have been carried out.

3.3. Spectroscopic Analysis. Table 6 is a compilation of vibrational term values and integrated absorption cross-sections in $^{14}NH_3$. Tables 7–9 collect vibrational term values for three isotopomers of ammonia. For the theoretical results from the present work, the following masses were used: 14.003074 u (N), 1.007825 u (H), 2.014102 u (D). The labeling and notation of vibrational levels follow recommendations[73,77,78] (see the footnotes for additional information). Symmetry labels are given with respect to the molecular symmetry group $\mathbf{M}_{s12}$, isomorphous to D_{3h}, in case of $^{14}NH_3$ and $^{14}ND_3$, and with respect to $\mathbf{M}_{s4}$ in case of $^{14}NH_2D$ and $^{14}NHD_2$ (see section 2.5).

Integrated absorption cross-sections in Table 6 were evaluated from the equation[79]

$$G_{fi} = \frac{8\pi^3}{3hc(4\pi\varepsilon_0)} |M_{fi}|^2 \approx 41.624 \left(\frac{|M_{fi}|}{\mathrm{D}} \right)^2 \mathrm{pm}^2 \quad (15)$$

Transition electric dipole moments M_{fi} were obtained within the DVR of wave functions calculated from AMMPOT4 (in column "this work"), and the dipole moment surfaces for ammonia from refs 40 and 55 or from published data (column "experiment"). The data in column YZLJT are from a yet unpublished evaluation of the PES from ref 38 using the TROVE program,[58] as described above. These data differ only slightly from those published previously,[15] which were obtained for a PES representation in which the equilibrium parameters were adjusted differently.

Table 6a gives a rather complete account of our present knowledge on the vibrational spectroscopy of NH_3 in the region up to 5000 cm^{-1}, which includes all fundamentals and the first few bending overtones up to the fifth overtone of the inversion mode. Here, we compare results obtained from selected previously published PES of ammonia with those obtained with AMMPOT4. Among these, the HSL-2 PES[16,43] yields with 1.22 cm^{-1}, the lowest root-mean-square deviation to the reported experimental band centers in this wavenumber range. We underline that the data in columns HSL-2 and RMH were obtained from a final adjustment of the analytical representation to the experimentally determined transitions in Table 6a. The other PESs discussed in Table 6 give rise to slightly larger deviations. Transitions using the RMH PES (acronyms as defined in ref 22) are from "fit I" in ref 14; the same fit is used for transitions reported in Table 6b, whereas in Table 6c the PES called "surface I" from ref 14 is used, which gives significantly less good results in the lower energy region reported in Table 6a.

The AMMPOT4 PES has clearly the largest deviation, which is, however, acceptable in view of the small number of adjustable parameters used, taking into account the global character of this representation. Of all terms below the stretching fundamentals, only the doublet of the (2^14^1) transition at around 2560 cm^{-1}

dx.doi.org/10.1021/jp4016728 | J. Phys. Chem. A 2013, 117, 7502–7522

Table 6. Experimental and Calculated Wavenumbers and Integrated Absorption Cross Sections for NH_3: (a) Wavenumber Range between 0 and 5000 cm^{-1}; (b) Wavenumber Range between 5000 and 8250 cm^{-1}; (c) Wavenumber Range above 8250 cm^{-1}

(a)

		experiment				theory					
						$\tilde{\nu}/(cm^{-1})$				this work (AMMPOT4)	
sym[a]	levels[b]	$\tilde{\nu}/(cm^{-1})$	ref	$G^{obs}/(pm^2)$	ref	HSL-2[43]	YZLJT[38n]	LCH[41]	RMH[14]	$\tilde{\nu}/(cm^{-1})$	$G^c/(pm^2)$
A_1^+	$(0)^l$	0.00				0.00	0.00	0.00	0.00	0.00	
A_2^-	$(0)^u$	0.79[m]	93	$0.90 \times 10^{+2}$	94	0.79	0.80	0.74	0.79	0.75	$0.88 \times 10^{+2}$
A_1^+	$(2^1)^l$	932.43[m]	93	$0.26 \times 10^{+1}$	95	932.44	932.96	933.78	932.23	932.27	$0.25 \times 10^{+1}$
A_2^-	$(2^1)^u$	968.12[m]	93	$0.23 \times 10^{+1}$	95	968.15	969.21	968.64	968.13	966.22	$0.23 \times 10^{+1}$
A_1^+	$(2^2)^l$	1597.47[m]	96	0.17×10^{-1}	96	1597.46	1596.81	1597.07	1597.91	1601.46	0.17×10^{-1}
E^+	$(4^1)^l$	1626.28	96	$0.14 \times 10^{+0}$	96	1626.28	1625.77	1628.81	1626.21	1628.45	$0.28 \times 10^{+0}$
E^-	$(4^1)^u$	1627.37	96	$0.13 \times 10^{+0}$	96	1627.37	1626.93	1629.81	1627.30	1629.33	$0.28 \times 10^{+0}$
A_2^-	$(2^2)^u$	1882.18[m]	96	0.44×10^{-3}	96	1882.14	1883.89	1881.45	1882.55	1878.99	0.35×10^{-3}
A_1^+	$(2^3)^l$	2384.15[m]	97	0.10×10^{-2}	97	2384.17	2386.17	2383.08	2385.42	2381.03	0.14×10^{-2}
E^+	$(2^14^1)^l$	2540.53	97	0.30×10^{-3}	97	2540.50	2535.82	2544.35	2540.30	2560.46	0.35×10^{-2}
E^-	$(2^14^1)^u$	2586.13	97	0.27×10^{-3}	97	2586.09	2583.79	2588.10	2586.08	2599.48	0.36×10^{-2}
A_2^-	$(2^3)^u$	2895.51[m]	97	0.34×10^{-3}	97	2895.52	2898.92	2896.19	2895.59	2888.81	0.58×10^{-3}
A_1^+	$(4^{2,0})^l$	3216.10[m]	98	*k*	83	3215.94	3213.05	3221.17	3216.61	3220.87	0.18×10^{-2}
A_2^-	$(4^{2,0})^u$	3217.78[m]	98	*k*	83	3217.57	3214.89	3222.93	3218.28	3222.09	0.19×10^{-2}
E^+	$(2^24^1)^l$	*d*		*d*		3189.62	3180.11	*d*	*d*	3222.53	0.25×10^{-7}
E^-	$(4^{2,2})^l$	3240.44[e]	98	*k*	83	3240.16[e]	3237.99[e]	3244.66[e]	3240.61[e]	3246.87	0.35×10^{-2}
E^+	$(4^{2,2})^u$	3241.62[f]	98	*k*	83	3241.59[f]	3239.54[f]	3245.89[f]	3242.03[f]	3248.73	0.39×10^{-2}
A_1^+	$(1^1)^l$	3336.11[m]	98	0.29×10^{-1}	83	3336.10	3341.87	3335.13	3338.87	3334.73	0.29×10^{-1}
A_2^-	$(1^1)^u$	3337.09[m]	98	0.29×10^{-1}	83	3337.08	3342.92	3336.49	3340.10	3335.61	0.29×10^{-1}
E^+	$(3^1)^l$	3443.63	98	0.14×10^{-1}	83	3443.63	3446.68	3442.16	3443.36	3445.85	0.16×10^{-1}
E^-	$(3^1)^u$	3443.99	98	0.14×10^{-1}	83	3443.99	3447.04	3442.51	3443.71	3445.99	0.16×10^{-1}
A_1^+	$(2^4)^l$	3462.00[m]	99	*d*		3462.48	3466.94	3466.52	3460.85	3453.08	0.16×10^{-3}
E^-	$(2^24^1)^u$	*d*		*d*		3502.57	3499.79	*d*	*d*	3521.42	0.49×10^{-4}
E^+	$(2^34^1)^l$	*d*		*d*		4007.78	4005.01	*d*	*d*	4028.24	0.21×10^{-5}
A_2^-	$(2^4)^u$	4055.00[m]	100	*d*		4061.78	4067.22	4068.42	4055.31	4051.12	0.94×10^{-5}
A_1^+	$(2^14^{2,0})^l$	4115.62	101	*d*		4115.85	4097.08	4123.40	4115.99	4134.41	0.51×10^{-3}
E^+	$(2^14^{2,2})^l$	4135.94	101	*d*		4136.00	4122.31	*d*	4136.33	4167.56	0.48×10^{-3}
A_2^-	$(2^14^{2,0})^u$	4173.25	101	*d*		4173.14	4162.46	4178.62	4173.60	4184.40	0.73×10^{-3}
E^-	$(2^14^{2,2})^u$	4193.14	101	*d*		4193.06	4185.21	*d*	4193.54	4214.31	0.58×10^{-3}
A_1^+	$(1^12^1)^l$	4294.53	101	0.26×10^{-2}	102	4294.51	4301.09	4296.00	4291.42	4274.07	0.41×10^{-2}
A_2^-	$(1^12^1)^u$	4320.04	101	0.26×10^{-2}	102	4320.01	4326.98	4321.23	4320.22	4302.87	0.37×10^{-2}
E^+	$(2^13^1)^l$	4416.91	101	0.18×10^{-1}	102	4416.92	4420.79	4419.06	4419.18	4408.98	0.26×10^{-1}
E^-	$(2^13^1)^u$	4435.44	101	0.18×10^{-1}	102	4435.44	4439.64	4436.92	4437.81	4427.91	0.26×10^{-1}
E^-	$(2^34^1)^u$	*d*		*d*		4530.72	4530.59	*d*	*d*	4548.35	0.28×10^{-4}
A_1^+	$(2^5)^l$	*d*		*d*		4694.73	4700.10	*d*	*d*	4681.68	0.98×10^{-6}
A_1^+	$(2^24^{2,0})^l$	*d*		*d*		4757.46	4728.95	*d*	*d*	4786.66	0.23×10^{-4}
E^+	$(4^{3,1})^l$	*d*		*d*		4799.14	4791.97	*d*	*d*	4796.16	0.78×10^{-4}
E^-	$(4^{3,1})^u$	*d*		*d*		4801.21	4794.39	*d*	*d*	4799.83	0.93×10^{-4}
E^+	$(2^24^{2,2})^l$	*d*		*d*		4774.60	4752.67	*d*	*d*	4827.17	0.20×10^{-4}
A_1^+	$(4^3)^l$	*d*		*d*		4841.81	4836.27	*d*	*d*	4843.14	0.22×10^{-12}
A_2^-	$(4^3)^u$	*d*		*d*		4843.58	4838.21	*d*	*d*	4844.88	0.21×10^{-12}
A_1^-	$(4^3)^l$	*d*		*d*		*d*	4836.67[e]	*d*	*d*	4854.00	0.77×10^{-5}
A_2^+	$(4^3)^u$	*d*		*d*		*d*	4839.01[f]	*d*	*d*	4856.76	0.18×10^{-4}
E^+	$(1^14^1)^l$	4955.85	82	*d*		4955.74	4960.21	4957.71	4959.55	4949.59	0.14×10^{-3}
E^-	$(1^14^1)^u$	4956.79	82	*d*		4956.90	4961.50	4959.05	4960.90	4950.52	0.13×10^{-3}
		$\Delta\tilde{\nu}_{rms}$[l]/cm^{-1}				1.22	6.25	3.89	1.53	10.99	
				Δ^2_{log}[g]							0.15

(b)

		experiment		theory					
				$\tilde{\nu}/(cm^{-1})$				this work (AMMPOT4)	
sym[a]	levels[b]	$\tilde{\nu}/(cm^{-1})$	ref	HSL-2[43]	YZLJT[38n]	LCH[41]	RMH[14]	$\tilde{\nu}/(cm^{-1})$	$G^c/(pm^2)$
E^+	$(3^14^1)^l$	5052.60	82	5052.64	5054.96	5055.48	5052.11	5054.06	0.12×10^{-1}
E^-	$(3^14^1)^u$	5052.97	82	5053.24	5055.62	5056.04	5052.67	5054.42	0.12×10^{-1}

dx.doi.org/10.1021/jp4016728 | J. Phys. Chem. A 2013, 117, 7502−7522

Table 6. continued

(b)

		experiment		theory				this work (AMMPOT4)	
				$\tilde{\nu}/(cm^{-1})$					
sym[a]	levels[b]	$\tilde{\nu}/(cm^{-1})$	ref	HSL-2[43]	YZLJT[38 n]	LCH[41]	RMH[14]	$\tilde{\nu}/(cm^{-1})$	$G^c/(pm^2)$
E^+	$(2^1 3^1 4^1)^l$	6012.90	82	6012.68	6011.86	*d*	6014.91	6018.66	0.66×10^{-3}
E^-	$(2^1 3^1 4^1)^u$	6037.12	82	6036.31	6036.92	*d*	6038.65	6040.83	0.67×10^{-3}
A^+	$(^o)^l$	6520.00[i]	82	6520.08	6520.09	*d*	6529.40	6512.89	0.22×10^{-4}
A^-	$(^o)^u$	6520.00[i]	82	6521.77	6522.01	*d*	6531.56	6514.09	0.21×10^{-4}
E^+	$(1^1 4^{2,2})^l$	6556.42	85	6556.80	6557.18	*d*	6562.94	6545.01	0.24×10^{-3}
E^-	$(1^1 4^{2,2})^u$	6557.93	85	6558.22	6559.08	*d*	6564.68	6547.89	0.30×10^{-3}
E^+	$(1^1 2^1 4^1)^l$	*d*		6580.98	6576.08	*d*	*d*	6570.50	0.12×10^{-3}
A^+	$(^o)^l$	6606.00[i]	82	6605.66	6605.75	*d*	6617.15	6614.11	0.72×10^{-6}
A^-	$(^o)^u$	6606.00[i]	82	6606.63	6606.83	*d*	6618.53	6615.00	0.58×10^{-6}
E^+	$(^P)^l$	6608.15	85	6610.29	6608.88	*d*	6614.87	6612.29	0.23×10^{-2}
E^-	$(^P)^u$	6609.72	85	6611.22	6609.86	*d*	6615.93	6612.65	0.24×10^{-2}
E^-	$(3^1 4^2)^l$	6665.30	81	6665.77	6663.14	*d*	*d*	6663.55	0.10×10^{-2}
E^+	$(3^1 4^2)^u$	6666.70	81	6666.24	6665.98	*d*	*d*	6663.56	0.11×10^{-2}
E^-	$(^P)^l$	6680.93[e,r]	81	6679.25[e]	6677.43[e]	*d*	6665.40[e]	6682.14	0.27×10^{-2}
E^+	$(^P)^u$	6681.87[f,r]	81	6679.36[f]	6678.33[f]	*d*	6665.92[f]	6682.19	0.26×10^{-2}
A^-	$(^o)^l$	6795.46	86	6796.52	6792.28[e]	*d*	6810.67	6807.92	0.28×10^{-3}
A^+	$(^o)^u$	6795.96	86	6797.91	6796.46[f]	*d*	6812.36	6808.45	0.27×10^{-3}
E^-	$(^P)^l$	6850.20[e]	81	6850.46[e]	6855.52[e]	*d*	6847.72[e]	6864.78	0.35×10^{-3}
E^+	$(^P)^u$	6850.65[f]	81	6850.86[f]	6855.99[f]	*d*	6848.12[f]	6865.76	0.30×10^{-3}
E^+	$(^P)^l$	*d*		7659.59	7654.07	*d*	*d*	7645.51	0.37×10^{-3}
E^-	$(^P)^u$	*d*		7676.09	7671.76	*d*	*d*	7663.65	0.32×10^{-3}
E^+	$(^q)^l$	*d*		8176.18	8171.35	*d*	*d*	8174.18	0.61×10^{-4}
E^-	$(^q)^u$	*d*		8177.64	8173.07	*d*	*d*	8175.08	0.62×10^{-4}
E^+	$(^q)^l$	8200.00[i]	82	8208.83	8203.03	*d*	8218.45	8209.03	0.15×10^{-4}
E^-	$(^q)^u$	8200.00[i]	82	8208.32	8204.49	*d*	8219.78	8209.92	0.15×10^{-4}
E^+	$(^q)^l$	*d*		8284.86	8281.77	*d*	*d*	8273.91	0.19×10^{-3}
E^-	$(^q)^u$	*d*		8286.05	8283.48	*d*	*d*	8274.16	0.21×10^{-3}
		$\Delta\tilde{\nu}_{rms}{}^l/cm^{-1}$		2.59	2.59	2.98	11.00	8.15	

(c)

		experiment		theory			this work (AMMPOT4)	
				$\tilde{\nu}/(cm^{-1})$				
sym[a]	levels[b]	$\tilde{\nu}/(cm^{-1})$	ref	HSL-0[36]	YZLJT[38 n]	RMH[14]	$\tilde{\nu}/(cm^{-1})$	$G^c/(pm^2)$
E^+	$(1^2 4^2)^l$	9639.65	82	9645.30	9624.74[e]	9647.14[e]	9671.36	0.27×10^{-5}
E^-	$(1^2 4^2)^u$	9642.32	82	*d*	9629.87[f]	9649.28[f]	9671.96	0.23×10^{-5}
E^+	$(1^2 3^1)^l$	9689.72	82	9694.00	9676.12	9692.68	9704.06	0.27×10^{-8}
E^-	$(1^2 3^1)^u$	9689.84	82	*d*	9678.00	9694.76	9705.75	0.27×10^{-8}
E^+	$(3^2 4^2)^l$	9738.15	82	9740.70	9721.82	9740.12	9748.99	0.22×10^{-3}
E^-	$(3^2 4^2)^u$	9738.84	82	*d*	9723.43	9741.53	9749.79	0.22×10^{-3}
E^+	$(1^1 3^1 4^2)^l$	10066.00[i]	82	*d*	10043.03	*d*	10064.85[i]	0.72×10^{-5i}
E^-	$(1^1 3^1 4^2)^u$	10066.00[i]	82	*d*	10043.71	*d*	10064.85[i]	0.72×10^{-5i}
E^+	$(1^1 3^2)^l$	10110.86	82	10111.60[s]	10106.42	10111.06	10143.15[i]	0.50×10^{-5i}
E^-	$(1^1 3^2)^u$	10111.31	82	10112.40[s]	10107.31	10111.55	10143.15[i]	0.50×10^{-5i}
A^-	$(3^3)^l$	10232.52[e]	82	10233.20[s]	10237.50	10231.54[e]	10271.05[i]	0.86×10^{-6i}
A^+	$(3^3)^u$	10234.73[f]	82	10236.70[s]	10238.50	10231.71[f]	10271.05[i]	0.86×10^{-6i}
E^j	*h*	12628.20[i]	82	*d*	*d*	*d*	*d*	*d*
E^+	$(1^3 3^{1,1})^l$	12675.5[i]	82	*d*	*d*	*d*	*d*	*d*
E^-	$(1^3 3^{1,1})^u$	12675.5[i]	82	*d*	*d*	*d*	*d*	*d*
A^+	$(1^5)^l$	15447.38	82	*d*	*d*	15442.47[e]	*d*	*d*
E^-	$(1^4 3^{1,1})^l$	15448.70	82	*d*	*d*	15442.80	*d*	*d*
A^-	$(1^5)^u$	15450.82	82	*d*	*d*	15445.42[f]	*d*	*d*

dx.doi.org/10.1021/jp4016728 | J. Phys. Chem. A 2013, 117, 7502−7522

Table 6. continued

(c)

		experiment		theory				
				$\tilde{\nu}/(cm^{-1})$			this work (AMMPOT4)	
sym[a]	levels[b]	$\tilde{\nu}/(cm^{-1})$	ref	HSL-0[36]	YZLJT[38] [n]	RMH[14]	$\tilde{\nu}/(cm^{-1})$	$G^c/(pm^2)$
E^+	$(1^4 3^{1,1})^u$	15451.19	82	*d*	*d*	15446.29	*d*	*d*
		$\Delta\tilde{\nu}_{rms}$ [l]$/cm^{-1}$		3.00	13.86	4.40	24.90	

[a]Symmetry according to wave functions determined in this work; labels are defined in Table 3 (see section 2.5); 1 and 2 subscripts are given in Table 6a, but omitted later. [b]Level assignments from the analysis of wave functions determined in this work, where available; all else from ref 37; assignments indicate the most important normal mode product state; when such a clear attribution is not possible, i.e., due to a very strong mixing of modes in the wave function, no attribution is given (see also text). [c]*G* gives transition starting either from 0^l (A^+) (E^+, $A^- \leftarrow A^+$) or from 0^u (A^-) (E^-, $A^+ \leftarrow A^-$). Wave functions based on AMMPOT4 dipole moment surfaces from refs 40 (Tables 6a,b) and 55 (Table 6c). [d]Not measured or not calculated. [e]A^+ or E^+ symmetry in the original article. [f]A^- or E^- symmetry in the original article. [g]$\Delta^2_{log} = (1/(n_{dat}))\Sigma_{i=1}^{n_{dat}}(\log_{10}[(G_i^{th})/(G_i^{exp})])^2$. [h]Lower or upper component not resolved. [i]Tunneling components not resolved. [j]Symmetry species not resolved. [k]The sum of the ($l_4 = 0$) $A^+ \leftarrow A^-$ and ($l_4 = 2$) $E^+ \leftarrow A^+$ band absorption cross-sections is reported in ref 83 to be 0.35×10^{-2} pm^2. [l]$\Delta\tilde{\nu}_{rms}$ is the root-mean-square deviation between experimental and theoretical wavenumbers within the same page in the table. [m]These 13 bands were used for a quick evaluation of vibrational transitions with the MULTIMODE program in a preliminary adjustment step (see text). [n]Data from a new calculation of vibrational term values using the CBS**4 ab initio potential energy surface from ref 38 (see text). [o]Strongly mixed state with major component 1^2 or $3^{2,0}$. [p]Strongly mixed state with major component $3^{2,2}$ or $1^1 3^1$. [q]Strongly mixed state with major component $1^2 4^1$ or $3^2 4^1$. [r]In ref 87, the values 6676.30 and 6676.81 cm^{-1} are reported. [s]In ref 43, the values 10114.44 and 10115.22 cm^{-1} as well as 10234.31 and 10236.56 cm^{-1} are reported, respectively, for the $1^1 3^2$ and 3^3 levels.

deviates by about 20 cm^{-1} from the experimental values. The vibrational term values obtained from an evaluation of the global PES developed in ref 33 show significantly larger deviations.[80] Also, the harmonic wavenumbers reported on the recently published representations of the $\tilde{X}$ and $\tilde{A}$ states of ammonia[32] deviate significantly from experimental estimates.

Regarding vibrational spectroscopy, the probably best currently available PES of ammonia are the NH3-Y2010 PES[17] and the HSL-2 PES.[16,43] These representations are experimentally refined polynomial expressions, which reproduce selected experimental ro-vibrational term values for $J = 0$, 1, 2, 3, 5, and 8 to within better than 0.2 cm^{-1} (0.02 cm^{-1} in ref 43). The NH3-Y2010 PES reproduces the positions of vibrational band centers above 6500 cm^{-1} slightly better than the HSL-2 PES. Some of the data reported in ref 43 were used in ref 81 for new determinations and assignments of band centers in the region between 6300 and 7000 cm^{-1}, which were previously reported in ref 82. In Table 6, these new values have been taken into account.

Absolute integrated absorption cross-sections agree well with available experimental data. We also evaluated transition dipole moments using a previously developed dipole moment operator for ammonia,[55] but the agreement is slightly less good (logarithmic root-mean-square deviation $\Delta^2_{log} = 1.03$ for the data in Table 6a, instead of 0.15 obtained for the dipole moment surface from ref 40). We note here that, following ref 83, the 1^1 and $4^{2,l=0}$ levels are strongly coupled by a Fermi resonance, but the authors of that article do not give band centers for these transitions. In the current table, we adopt experimental term values as given in ref 84.

Experimental information on some higher lying overtones and combination bands between 4400 and 5000 cm^{-1} are still missing. We give, in column "this work", both the expected line position and intensity from the present calculation, the former of which should be accurate to within ±10 to 20 cm^{-1}. Some of the lower combination bands have not yet been assigned experimentally, although the expected absorption cross-sections indicate that they should be observable.

Table 6b summarizes spectroscopic data for NH_3 between 5000 and 8250 cm^{-1}. Known data are sparser in this wavenumber range, as marked by footnote d in the table. Empty pairs of parentheses indicate levels where a clear attribution of the most important overtone or combination band contributing to that level is not possible. When compared to the range below 5000 cm^{-1}, the root-mean-square deviation for the YZLJT PES is smaller by a factor of 2, while that for the RMH PES increases by a factor of 4 ("fit I" PES from ref 14); for the PES from the present work, it has the same size. It is interesting to note that band centers from the purely ab initio YZLJT PES exhibit similar deviations, on average, as the HSL-2 PES, in this energy range. The LCH PES has a limited range of calculated vibrational levels and is not considered further. This table shows the adequacy of AMMPOT4 to reproduce vibrational term values up to 8000 cm^{-1} in a quite satisfactory way. We note that, here too, some levels have not yet been observed or assigned experimentally, although the expected intensity should allow for their observation. No experimental value is reported for absolute absorption cross-sections in this wavenumber range. Relative band strengths agree with approximative estimations from ref 82. We note that theoretical term values obtained with the PES "surface I" from ref 14 agree better with experimental values in this region. However, that PES yields values in the lower part of the spectrum that agree rather poorly with experimental values. In the spirit of discussing global representations of potential energy surfaces, we find it justified to compare here values resulting from the same PES.

The 1.5 μm region hosts states of the polyad $N = 2$. The polyad quantum number N defines the subset of normal mode product states involving v_s quanta of stretching and v_b quanta of bending modes, such that $v_s + v_b/2 = N$. In NH_3 or ND_3, the following combinations fall in the polyad $N = 2$:4^4, $1^1 4^2$, $3^1 4^2$, 1^2, 3^2 (of A_1 type in C_{3v}), $3^1 4^2$ (A_2), and 4^4 (2×), $1^1 4^2$, $3^1 4^2$ (2×), $1^1 3^1$, 3^2 (E). Other combinations such as $1^2 2^2 4^1$ might also fall in this spectral range. Table 6b reports only a subset of these states, and in the experimental work cited there, transitions were sometimes assigned to normal mode product states after analysis of rotational sublevels.

The observation of the band leading to the term at 6606 cm^{-1} is only marginally documented in ref 82. We find that, indeed, the absorption cross-section for this band should be very small. Yet, it is uncertain whether this term can be assigned to the 1^1 or any other A_1 type combination from the above list. In ref 43, this level is about 75% 1^1; in ref 17, it is assigned as $1^1 4^{2,0}$. With AMMPOT4, the close lying E-type level turns out to be lower than the A-type level, which is an inaccuracy of this analytical representation.

The E-type level at 6608 cm^{-1} may be assigned to the $1^1 3^{1,1}$ normal mode combination from a detailed analysis of ro-vibrational lines. In ref 85, there is experimental evidence that this level has an almost pure

dx.doi.org/10.1021/jp4016728 | J. Phys. Chem. A 2013, 117, 7502−7522

Table 7. Experimental and Calculated Wavenumbers $\tilde{\nu}_n$ (cm^{-1}) for NH_2D

		experiment		theory		
sym[a]	levels[b]	$\tilde{\nu}/(cm^{-1})$	ref	RMH[14]	YZLJT[38 d]	AMMPOT4
A^+	$(0)^l$	0.00		0.00	0.00	0.00
A^-	$(0)^u$	0.406	103	0.40	0.41	0.38
A^+	$(2^1)^l$	876.37	103	876.37	877.04	875.68
A^-	$(2^1)^u$	896.56	103	896.56	897.59	894.70
B^+	$(4_b^1)^l$	1389.91	89, 108	1389.78	1389.83	1392.16
B^-	$(4_b^1)^u$	1390.50	89, 108	1390.36	1390.44	1392.62
A^+	$(2^2)^l$	c		1510.74	1510.16	1514.52
A^-	$(4_a^1)^l$	1591.00	89, 108	1590.72	1590.82	1590.76
A^+	$(4_a^1)^u$	1605.64	89, 108	1605.62	1605.35	1607.25
A^-	$(2^2)^u$	c		1736.68	1738.01	1734.85
A^+	$(2^3)^l$	c		2180.92	2181.40	2179.03
B^+	$(2^1 4_b^1)^l$	c		c	2244.02	2264.15
B^-	$(2^1 4_b^1)^u$	c		c	2272.49	2286.72
A^-	$(2^1 4_a^1)^l$	c		c	2467.64	2483.93
A^+	$(2^1 4_a^1)^u$	c		c	2474.68	2485.42
A^-	$(1^1)^l$	2505.90	89	2504.64	2510.84	2507.18
A^+	$(1^1)^u$	2506.51	89	2505.50	2511.34	2507.33
A^-	$(2^3)^u$	c		2642.93	2645.14	2639.60
A^+	$(4_b^2)^l$	c		c	2769.35	2776.31
A^-	$(4_b^2)^u$	c		c	2770.36	2777.01
B^+	$(2^1 4_b^1)^l$	c		c	2851.18	2894.86
B^-	$(4_a^1 4_b^1)^l$	c		c	2971.43	2978.53
B^+	$(4_a^1 4_b^1)^u$	c		c	2981.81	2987.12
A^+	$(2^4)^l$	c		c	3044.63	3066.18
B^-	$(2^1 4_b^1)^u$	c		c	3107.37	3125.11
A^+	$(4_a^2)^l$	c		c	3152.45	3149.59
A^-	$(4_a^2)^u$	c		c	3159.77	3163.61
A^+	$(2^1 4_a^1)^l$	c		c	3191.30	3214.17
A^-	$(2^1 4_a^1)^u$	c		c	3328.68	3347.42
A^+	$(3_a^1)^l$	3365.24	89	3359.68	3370.91	3361.19
A^-	$(3_a^1)^u$	3367.59	89	3363.30	3373.02	3365.24
A^+	$(1^1 2^1)^l$	c		c	3417.55	3406.08
A^-	$(1^1 2^1)^u$	c		c	3429.00	3417.86
B^+	$(3_b^1)^l$	3438.86	89	3439.13	3442.09	3442.41
B^-	$(3_b^1)^u$	3439.03	89	3439.30	3442.28	3442.67
A^-	$(2^4)^u$	c		c	3671.01	3656.48
A^+	$(2^5)^l$	c		c	4226.71	4213.01
A^-	$(2^5)^u$	c		c	4820.35	4790.09
		$\Delta\tilde{\nu}_{rms}/cm^{-1}$		2.00	3.19	2.26

[a]Symmetry in the $\mathbf{M}_{s4}$ molecular symmetry group according to wave functions determined in this work; symmetry labels correlate to labels of the isomorphic C_{2v} group as follows:

$\mathbf{M}_{s4}$	A^+	A^-	B^+	B^-
$\mathbf{C}_{2v}$	A_1	A_2	B_2	B_1

In this table, B_2 is the symmetric representation upon reflection at the molecular plane at planar configurations. [b]Level assignments from the analysis of wave functions determined in this work; the spectroscopic notation of vibrational modes follows the proposition made in ref 88 if modes are classified following the C_{2v} point group (at planar configuration), the present mode notation correlates with the notation recommended in refs 77 and 78 as follows:

$\tilde{\nu}/cm^{-1} \sim$	3365	2506	1591	876	3439	1390
$\mathbf{C}_{2v}$	A_1	A_1	A_1	B_1	B_2	B_2
following[78]	1	2	3	4	5	6
following[88]	3_a	1	4_a	2	3_b	4_b

Assignments indicate the most important normal mode product overtone or combination level contributing to the vibrational level. [c]Not measured or not calculated. [d]Data from a new calculation of vibrational term values using the CBS**4 ab initio potential energy surface from ref 38 (see text).

dx.doi.org/10.1021/jp4016728 | J. Phys. Chem. A 2013, 117, 7502−7522

Table 8. Experimental and Calculated Wavenumbers $\tilde{\nu}_n$ (cm^{-1}) for NHD_2

		experiment		theory		
sym[a]	levels[b]	$\tilde{\nu}/(cm^{-1})$	ref	RMH[14]	YZLJT[38,f]	AMMPOT4
A^+	$(0)^l$	0.00	104	0.00	0.00	0.00
A^-	$(0)^u$	0.171	104	0.17	0.176	0.16
A^+	$(2^1)^l$	810.23	104	810.22	811.01	808.81
A^-	$(2^1)^u$	819.56	104	819.58	820.54	817.52
A^+	$(4_a^1)^l$	1233.37	88, 108	1233.11	1233.49	1234.29
A^-	$(4_a^1)^u$	1235.89	88, 108	1235.65	1236.06	1236.71
A^+	$(2^2)^l$	c		1445.05	1444.66	1449.68
B^+	$(4_b^1)^l$	1461.79	88, 108	1461.57	1461.86	1461.48
B^-	$(4_b^1)^u$	1461.99	88, 108	1461.78	1462.09	1461.65
A^-	$(2^2)^u$	c		1576.49	1577.98	1575.11
A^+	$(2^3)^l$	c		1952.23	1952.02	1956.48
A^-	$(2^1 4_a^1)^l$	c		c	2035.56	2044.85
A^+	$(2^1 4_a^1)^u$	c		c	2071.20	2080.45
B^+	$(2^1 4_b^1)^l$	c		c	2266.78	2280.21
B^-	$(2^1 4_b^1)^u$	c		c	2278.84	2289.13
A^-	$(2^3)^u$	c		2362.50	2364.88	2360.67
A^+	$(3_a^1)^l$	2430.80	88	2430.11	2433.32	2435.43
A^-	$(3_a^1)^u$	2434.62	88	2434.07	2437.78	2437.09
A^+	$(4_a^2)^l$	c		c	2482.53	2480.59
A^-	$(4_a^2)^u$	c		c	2486.76	2484.17
B^+	$(3_b^1)^l$	2559.81	88	2557.99	2563.59	2564.11
B^-	$(3_b^1)^u$	2559.96	88	2558.14	2563.77	2564.22
A^+	$(2^2 4_a^1)^l$	c		c	2620.25	2648.12
B^+	$(4_a^1 4_b^1)^l$	c		c	2691.66	2692.31
B^-	$(4_a^1 4_b^1)^u$	c		c	2695.12	2695.28
A^-	$(2^2 4_a^1)^u$	c		c	2793.17	2807.87
A^+	$(2^4)^l$	c		c	2811.40	2813.14
A^+	$(4_b^2)^l$	c		c	2885.31	2910.05
A^-	$(4_b^2)^u$	c		c	2906.78	2910.33
B^+	$(2^2 4_b^1)^l$	c		c	2907.26	2928.78
B^-	$(2^2 4_b^1)^u$	c		c	3036.06	3057.17
A^-	$(2^4)^u$	c		c	3260.01	3253.86
A^-	$(1^1)^l$	3404.24[d]	88	3407.10[d]	3408.70[d]	3406.27
A^+	$(1^1)^u$	3404.32[e]	88	3407.35[e]	3408.84[e]	3406.33
A^+	$(2^5)^l$	c		c	3725.03	3718.95
A^-	$(2^5)^u$	c		c	4217.94	4211.34
		$\Delta\tilde{\nu}_{rms}/cm^{-1}$		1.39	2.59	2.48

[a]Symmetry in the $\mathbf{M}_{s4}$ molecular symmetry group according to wave functions determined in this work; symmetry labels correlate to labels of the isomorphic C_{2v} group as in the caption to Table 7. [b]Level assignments from the analysis of wave functions determined in this work; spectroscopic notation as described in Table 7; if modes are classified following the C_{2v} point group (at planar configuration), the present mode notation correlates with the notation recommended in refs 77 and 78 as follows:

$\tilde{\nu}/cm^{-1} \sim$	3404	2431	1233	810	2560	1462
$\mathbf{C}_{2v}$	A_1	A_1	A_1	B_1	B_2	B_2
following[78]	1	2	3	4	5	6
following[88]	1	3_a	4_a	2	3_b	4_b

Assignments indicate the most important normal mode overtone or combination level contributing to the vibrational level. [c]Not measured or not calculated. [d]A^+ symmetry in the original article. [e]A^- symmetry in the original article. [f]Data from a new calculation of vibrational term values using the CBS**4 ab initio potential energy surface from ref 38 (see text).

vibrational angular momentum $l = 1$. However, this value is also compatible with the $3^1 4^{2,0}$ combination, or some combination involving the inversion mode, like $3^{2,0}2^2 4^{1,1}$.

A similar result is obtained for the E-type level at 6795 cm^{-1}, which may be assigned to the $3^{2,0}$ normal mode overtone.[86] However, criteria based on l-doubling may also lead to the assignment 1^2 or $1^2 4^{2,0}$. We find that all states in this region show rather strong mixing of many normal mode overtone or combination levels, while in ref 43 this level is assigned as $3^{2,0}$, in agreement with ref 86. From our calculations we obtain many close lying levels in this region, but only those reported in Table 6b have large transition cross-sections. In agreement with experiment, and the HSL-2 PES, we find that the wave function assigned to the term value at 6795.96 cm^{-1} is symmetric with respect to inversion, while the YZLJT PES yields a symmetric lower component for this doublet. We should note that in ref 17 this level was excluded from the fit.

dx.doi.org/10.1021/jp4016728 | J. Phys. Chem. A 2013, 117, 7502−7522

Table 9. Experimental and Calculated Wavenumbers $\tilde{\nu}_n$ (cm^{-1}) for ND_3

		experiment		theory		
sym[a]	levels[b]	$\tilde{\nu}/(cm^{-1})$	ref	RMH[14]	YZLJT[38 g]	AMMPOT4
A_1^+	$(0)^l$	0.00		0.00	0.00	0.00
A_2^-	$(0)^u$	0.053	105	0.05	0.054	0.05
A_1^+	$(2^1)^l$	745.60	105	745.72	746.42	743.47
A_2^-	$(2^1)^u$	749.14	105	749.27	750.05	746.76
E^+	$(4^1)^l$	1191.49	105	1190.26	1190.85	1189.76
E^-	$(4^1)^u$	1191.56	105	1190.33	1190.93	1189.81
A_1^+	$(2^2)^l$	1359.00	69	1358.62	1358.80	1361.00
A_2^-	$(2^2)^u$	1429.00	69	1429.60	1431.16	1427.51
A_1^+	$(2^3)^l$	1830.00	69	1826.78	1826.46	1829.08
E^+	$(2^14^1)^l$	*c*		1930.52	1930.29	1939.94
E^-	$(2^14^1)^u$	*c*		1634.96[d]	1934.98	1943.34
A_2^-	$(2^3)^u$	2106.60	69	2106.56	2108.80	2102.91
A_1^+	$(4^{2,0})^l$	2359.00[i]	69	*c*	2355.74	2355.63
A_2^-	$(4^{2,0})^u$	2359.00[i]	69	*c*	2356.09	2355.70
E^+	$(4^{2,2})^l$	*c*		*c*	2375.34	2376.61
E^-	$(4^{2,2})^u$	*c*		*c*	2375.45	2376.69
A_1^+	$(1^1)^l$	2420.11	106	2418.58	2425.28	2415.75
A_2^-	$(1^1)^u$	2420.65	106	2419.12	2425.91	2416.14
A_1^+	$(2^4)^l$	2482.00	107	2480.58	2483.46	2475.33
E^+	$(2^24^1)^l$	*c*		*c*	2525.92	2559.12
E^-	$(3^1)^l$	2563.91[e]	106	2561.96[e]	2567.89	2563.95
E^+	$(3^1)^u$	2563.93[f]	106	2561.98[f]	2567.92	2564.39
E^-	$(2^24^1)^u$	*c*		*c*	2611.29	2628.54
A_2^-	$(2^4)^u$	2876.00	107	2869.96	2874.88	2863.60
E^+	$(2^34^1)^l$	*c*		*c*	2996.51	3030.01
A_1^+	$(1^12^1)^l$	3093.01	69	3092.04	3090.36	3103.53
A_2^-	$(1^12^1)^u$	3099.46	69	3097.84	3096.73	3107.30
E^+	$(2^14^{2,2})^l$	*c*		*c*	3107.29	3128.88
E^-	$(2^14^{2,2})^u$	*c*		*c*	3113.33	3132.14
A_1^+	$(2^14^{2,0})^l$	3171.89	84	3167.61	3178.20	3159.67
A_2^-	$(2^14^{2,0})^u$	3175.87	84	3171.96	3182.29	3163.48
A_1^+	$(2^5)^l$	*c*		*c*	3297.82	3282.55
E^-	$(2^34^1)^u$	*c*		*c*	3292.78	3308.93
E^+	$(2^13^1)^l$	3327.94	69	3327.80	3332.94	3321.57
E^-	$(2^13^1)^u$	3329.56	69	3329.44	3334.64	3323.62
E^+	$(3^14^1)^l$	*c*		3742.11	3748.34	3741.06
E^-	$(3^14^1)^u$	*c*		3742.14	3748.42	3741.73
E^+	$(1^13^1)^{lj}$	4887.29	69	4887.57	4892.53	4885.97
E^-	$(1^13^1)^{uj}$	4887.67	69	4888.01	4893.35	4886.04
E^-	$(3^14^2)^{lj}$	4938.44[i]	69	4939.21[e]	4942.94	4921.28
E^+	$(3^14^2)^{uj}$	4938.44[i]	69	4939.39[f]	4942.97	4921.59
E^+	$(3^{2,2})^{lj}$	5100.66[i]	69	5096.24[f]	5107.21	5105.27
E^-	$(3^{2,2})^{uj}$	5100.66[i]	69	5096.26[e]	5107.31	5105.32
		$\Delta\tilde{\nu}_{rms}$		2.30	4.01	7.13

[a]Symmetry according to wave functions determined in this work (see also caption to Table 6). [b]Level assignments from the analysis of wave functions determined in this work (see also caption to Table 6). [c]Not measured or not calculated. [d]Possibly a misprint in the original article. [e]A^+ or E^+ symmetry in the original article. [f]A^- or E^- symmetry in the original article. [g]Data from a new calculation of vibrational term values using the CBS**4 ab initio potential energy surface from ref 38 (see text). [i]Tunneling components not resolved. [j]Strongly mixed state in the polyad $N = 2$.

For the level at 6680 cm^{-1}, the experimentally determined ordering of "+" and "−" agrees with results from all PES, with the exception of AMMPOT4. We have checked that all calculated vibrational terms are numerically converged to within 0.1 cm^{-1} (tunneling splittings to at least 0.01 cm^{-1}). Remaining differences between values given under columns YZLJT and AMMPOT4, in particular in the "+" and "−" assignment of levels, originate thus from subtle differences between the underlying representations of the PES. In ref 87, the values 6676.30 and 6676.81 cm^{-1} were determined for this doublet, where it was concluded that analysis of *l*-doubling is insufficient to give a definite vibrational assignment to this level, too. The value reported in Table 6 is from a revised experimental determination of this level,[81] where new values are reported also for the level around 6666 cm^{-1}. We calculate that this level has a strong 3^14^2 component, as in ref 43, and an absorption cross-section that is only 1/3 of the level at 6680 cm^{-1}. From our calculations, we estimate that a larger number of vibrational levels should be

dx.doi.org/10.1021/jp4016728 | J. Phys. Chem. A 2013, 117, 7502−7522

experimentally accessible in the 1.5 μm region than what is known today. We do not report all results here, and additional information is available upon request. We just mention the perpendicular band leading to the level at around 7650 cm^{-1}, which should be as strong as the parallel band leading to the $3^{2,0}$ level.

The experimentally established term value 8200 cm^{-1} falls into the region of polyad N = 5/2, which involves at least the following normal mode product states: $3^2 4^1$ (A_1), $3^2 4^1$ (A_2), and $3^2 4^1$ (2×) (E). We obtain strong transitions for three levels, which we report in Table 6b and in which no normal mode combination dominates. We note that, according to our results, the reported experimental value should have an absorption cross-section that is a factor 10 smaller than the strongest transition reported for this region.

Table 6c summarizes spectroscopic data for NH_3 above 8250 cm^{-1}. Known experimental data are even sparser in this region, which involves the polyads N = 3, starting at 9500 cm^{-1}, polyad N = 4, at around 12 000 cm^{-1}, and polyad N = 5, starting at around 15 000 cm^{-1}. A large manifold of states is likely to be observed in absorption and, quite surprisingly, only a couple of bands are reported within each polyad. Because of a multitude of possible interacting states and the higher complexity of multidimensional calculations in this energy region, the assignment of levels to well-defined normal mode product states is highly uncertain. For instance, in ref 14, "surface I" therein, the assignments $1^1 4^4$ and $3^1 4^4$ are made for the states around 9650 and 9740 cm^{-1}, respectively, while we find the assignments $1^2 4^2$ and $3^2 4^2$ for the corresponding states. Reported transitions have rather strong absorption cross-sections ,which were evaluated, in Table 6c, from the dipole moment surface defined in ref 55.

The deviation of vibrational terms calculated from AMMPOT4 from known experimental values increases to above 50 cm^{-1} in the wavenumber range above 10 100 cm^{-1}. The YZLJT and RMH PES yield vibrational terms that agree remarkably well with experimental data also in the higher spectroscopic regions. As discussed above, the variational calculation of vibrational term values is highly complex and subject to a series of problems that are not always reported. The values reported for AMMPOT4 are accurate to within 20 cm^{-1} in the wavenumber range of Table 6c. We note also that a good quantitative description of vibrational terms does not necessarily imply that the PES is qualitatively good. The discussion carried out in ref 22 has for instance revealed that the RMH PES starts to deviate from a qualitatively correct asymptotic behavior for NH bond lengths of about 170 pm (see Figure 2 in ref 22), at a corresponding potential energy of 20 000 to 25 000 hc cm^{-1}. Because AMMPOT4 is a global representation of the PES, we think that it will allow for a better qualitative and quantitative description of molecular dynamics in the higher energy domain, despite the less pertinent quality of vibrational terms above 10 000 cm^{-1}.

Tables 7 and 8 summarize theoretical and experimental vibrational spectroscopic data for NH_2D and NHD_2[88,89] (see also ref 42). The agreement of term values obtained from AMMPOT4 with experimental and other theoretical values is acceptable, in the spirit of the discussion carried out above. Tunneling splittings are closer to experimental tunneling splittings than absolute term values. For instance, in the case of NHD_2, AMMPOT4 yields tunneling splittings that are significantly closer to experimental data than AMMPOT2, such as the splitting of the 1^1 doublet, which is 0.06 cm^{-1} with AMMPOT4 (0.08 cm^{-1} experimentally), whereas it is 3.72 cm^{-1} with AMMPOT2. We refrain from giving all data for AMMPOT2 here (some data were reported in ref 90) and note instead that the large value obtained with AMMPOT2 for the tunneling splitting of the ν_1-fundamental is at the origin of the fast tunneling motion found in ref 90, as confirmed in ref 91, where AMMPOT4 has been used. We should also note that the order of the A^+ and A^- levels of the NH stretching fundamental is inverted, in AMMPOT4, when compared to the experimentally determined values from ref 88, as well as with the theoretical values from refs 14 and 38.

Table 9 closes the summary and discussion of vibrational spectroscopic data issued from AMMPOT4. Results fall within the general trends of the analysis given above. In ref 43, it was concluded that vibrational term values obtained with the HSL-2 PES for ND_3 are less accurate than those for NH_3. Data obtained from the HSL-2 PES are not reproduced here.

4. CONCLUSIONS

In the present work, we have derived a new analytical representation for the lowest adiabatic potential energy surface (PES) of ammonia: AMMPOT4. The representation accounts for a global description of this hypersurface, as does the previously derived representation AMMPOT2;[22] the present representation is improved, with respect to the former one, from a quantitative point of view since it allows for the reproduction of the vibrational spectrum with significantly higher accuracy. This is the first global, full-dimensional representation of the lowest adiabatic potential energy surface of ammonia that is adequate for further use in quantum or classical dynamical calculations and that also approaches criteria of spectroscopic accuracy.

Our work presents also an overview and discussion of state-of-the-art results on ammonia vibrational spectroscopy, including band positions for all hydrogen and deuterated isotopomers and absorption cross-sections. All results are presented in a series of comparative tables with recent experimental and theoretical results based on: a PES representation obtained from a pure CCSD(T)/CBS** ab initio data set and fitted to a fourth order semiglobal local Taylor expansion;[38] the refinement procedure and comparative work of refs 36, 41, and 43; and the quartic order, local analytical representation derived from a tailored selection of ab initio point grids at the CCSD(T)/aug-cc-pVQZ level.[14] One conclusion from the review of presently available experimental data from high-resolution spectroscopy of ammonia is that, starting from the 1.5 μm region, further work is necessary in order to unravel the complicated structure of the vibrational spectra in the infrared to visible range. There are strong transitions falling in this region that have not yet been reported from experiment, to our knowledge.

For a more detailed description of the analytical form used in the present work as well as for details on the generic analytical form of PES representations of XY_n molecules, see refs 5, 7, 8, 22, and 92. AMMPOT4 has been obtained following a set of steps and techniques that we summarize as follows.

(1) The choice of appropriate ab initio data; the ab initio data are calculated using two different approaches, CCSD(T) and MRCI(SD). The CCSD(T) energies have been computed using CBS extrapolation to the complete basis set limit and have been used earlier[37,38] to cover the energy region from NH_3 equilibrium up to 20 000 hc cm^{-1}. This data set is optimal for describing the PES at geometries close to equilibrium. The MRCI(SD)/aug-cc-pVQZ energies are expected to give a good description of the PES in the asymptotic limits of NH bond dissociation.

(2) A new merging procedure; both data sets were connected to each other using a simple merging procedure, which involves an experimental estimate of the energy required for one NH bond dissociation ($D_e^{(exp)} \approx 41\,051$ hc cm^{-1}). In this procedure, no exact data matching is required, which is quite different from other

strategies.[25] The characteristic properties of compact analytical representations, such as *robustness* and *flexibility*, are found to be of fundamental importance in order to obtain a smoothly adjusted analytical representation when a merging procedure of multiple ab initio data sets is involved.

(3) An adjustment procedure based on the Levenberg−Marquardt algorithm and a detailed multistep application thereof; the adjustment of the analytical representation to the merged ab initio data set occurred in different steps and was combined with further graphical and numerical analysis of intermediate results and subsequent refinement using experimental data, either by inclusion of analytical expressions of parameters that model directly or indirectly observable quantities (for example, a simple bond dissociation energy) in a modified Levenberg−Marquardt algorithm[62] or by manual variation of certain parameters that influence significantly an experimental outcome, such as transition frequencies. Adjustment procedures that were refined by inclusion of experimental data have been used in the past.[7,11,38]

(4) A compact representation[7,92] built from generic functional forms; only 31 parameters are needed in this work (accounting for the domain of definition of bound NH_3), which is significantly less than used in other representations (84 in ref 37; 91 in ref 41; and 812 in ref 14). The analytical representation is fully symmetric with respect to the permutation of identical atoms.

AMMPOT4 has the following characteristic features.

(1) Saddle point for inversion: the inversion barrier is 1774 hc cm^{-1}, in good agreement with other accurate results.[16,17,36,66,67]

(2) AMMPOT4 yields a good description of the dissociation channel in the higher energy domain where simple bond cleavage reactions occur. The description is not expected to reach full spectroscopic accuracy in the high energy domain, but it should at least be accurate enough to account for all effects pertaining to the dissociation reaction, eq 1, and the inverse recombination reaction, eq 12, at total collision energies up to 0.1 eV. The PES represented by AMMPOT4 is a single-valued representation of the lowest adiabatic state, but in the collision energy domain mentioned above, it is comparable to the improved two-sheet representation obtained in ref 33; AMMPOT4 should yield a thermochemistry of similar accuracy but should be more accurate spectroscopically and thus kinetically more relevant in the given energy domain.

(3) The lowest, spin-forbidden dissociation channel of eq 3 is described in a qualitative way; for the moment, we estimate the barrier for this reaction to be at around 38 500 hc cm^{-1} above the NH_3 minimum, which is close to the dissociation energy for this reaction; the reverse recombination reaction, eq 13, is therefore almost barrierless in our simplified picture; the rate of this reaction is then entirely determined by the spin−orbit coupling. In order to improve the representation of the PES from a quantitative point of view, more work is needed here for definite conclusions, which include spin−orbit interaction on a dense grid of triplet and singlet points. We mention that the two-sheet representation both in refs 31 and 33 does not describe this dissociation channel at all.

(4) The evaluation of AMMPOT4 with a full-dimensional, variational quantum dynamical method yields vibrational spectroscopic line positions for ammonia and its deuterated isotopomers (fundamentals and overtones up to 10 000 cm^{-1}) that are in acceptable agreement with experimental values. Agreement is only slightly inferior to that found in previous work[37,38] where an equivalent ab initio data set was used in the low energy domain up to about 15 000 hc cm^{-1}. With the exception of a few transitions, the average difference between theoretical and experimental line positions is roughly 5 cm^{-1}.

Larger differences occur in the higher energy region above 10 000 hc cm^{-1}, for two reasons. First, in this region MRCI data start to have an increasing influence on the shape of the PES representation; the expectedly lower quality of these ab initio data (compared with CCSD(T)) as well as their lower density infers on the quality of the analytical representation. However, the robustness of compact analytical representations like the present one might be advantageous in such a case since such representations need less parameters to be adjusted. Second, analytical representations that use a large number of parameters are more flexible and may thus result in a lower root-mean-square (rms) deviation from experimental data; the representations discussed in previous work[14,16,17,36−38,40,41] are more flexible than the present one, which essentially explains their lower values of rms deviations in the fit. Third, quantum methods used to calculate vibrational eigenstates from a given representation of the PES tend to be less accurate for high lying vibrational states.

As discussed previously, a good agreement of theorectical and experimental vibrational spectra can be misleading. For instance, in ref 14, the highest reported overtone transitions for ammonia around 15 400 cm^{-1} are only a few cm^{-1} away from the experimental values. The corresponding energy is roughly half the dissociation energy, yet we know that the analytical representation in ref 14 cannot describe dissociation correctly.

In summary, the present analytical representation AMMPOT4 of the lowest adiabatic PES of ammonia gives a good account of vibrational transitions and simultaneously guarantees a qualitatively and physically correct description of the first two dissociation channels. Clearly, further improvement of the overall description of thermochemical, kinetic, and spectroscopic properties of ammonia with single adiabatic potential energy surface is possible. Such an improvement can in principle be achieved by adding flexibility to the analytical forms, for instance, by increasing the order of the polynomial expansions used in the angular forms (see ref 22). This leads, however, to an increase of the number of fitted parameters. As discussed above, polynomial forms with quite a large number of parameters are necessary to represent extended data sets of ab initio energy points with small rms deviations. As indicated in section 3.2.3, additional ab initio data are needed to describe the lowest, spin-forbidden dissociation channel more properly. The adjustment procedure discussed here includes a series of intermediate steps, where manual, deliberate adjustments were necessary to improve the description of experimental data from vibrational spectroscopy. Ideally, such steps should be replaced by an automatic algorithm (inverse spectroscopic problem). While successful solutions to this problem exist for small molecules (see, e.g., ref 18), they are significantly more difficult to find for tetra- or penta-atomic molecules. In this sense, the present analytical representation is a highly promising candidate for a successful solution of the direct spectrocopic inversion problem in ammonia because of the low number of adjustable parameters. The empirically refined PES for methane[7] is an example for the strategy to be applied.

■ ASSOCIATED CONTENT

Supporting Information

Tables with coordinates and energy values of the points determined in this work at several levels of ab initio calculation as well as a listing of the FORTRAN routine defining the analytical representation AMMPOT4. This material is available free of charge via the Internet at http://pubs.acs.org.

AUTHOR INFORMATION

Corresponding Author

*(R.M.) E-mail: roberto.marquardt@unistra.fr. Fax: 0(033)3 68 85 15 89.

Notes

The authors declare no competing financial interest.

ACKNOWLEDGMENTS

We thank Csaba Fabri for computational checks. The work of R.M. is supported financially by a grant from the French Ministry of Research. S.Y. and W.T. are grateful for support from the European Commission through contract no. MRTN-CT-2004-512202, "Quantitative Spectroscopy for Atmospheric and Astrophysical Research" (QUASAAR). This work was also supported by Schweizerischer Nationalfonds, ETH Zürich, and ERC.

REFERENCES

(1) Murrell, J. N.; Carter, S.; Farantos, S. C.; Huxley, P.; Varandas, A. J. C. *Potential Energy Functions*; Wiley: New York, 1984.

(2) Schatz, G. C. In *Advances in Molecular Electronic Structure Theory*; Dunning, T. H., Jr., Ed.; JAI Press Inc.: Greenwich, CT, 1990; Vol. *1*, pp 85−127.

(3) Hollebeek, T.; Ho, T.-S.; Rabitz, H. Constructing Multidimensional Molecular Potential Energy Surfaces from ab Initio Data. *Annu. Rev. Phys. Chem.* **1999**, *50*, 537−570.

(4) Braams, B. J.; Bowman, J. M. Permutationally Invariant Potential Energy Surfaces in High Dimensionality. *Int. Rev. Phys. Chem.* **2009**, *28*, 577−606.

(5) Marquardt, R.; Quack, M. Global Analytical Potential Energy Surfaces for High-Resolution Molecular Spectroscopy and Reaction Dynamics. In *Handbook of High Resolution Spectroscopy*; Quack, M., Merkt, F., Ed.; John Wiley: Chichester, U.K., 2011; Chapter 13, pp 511−550.

(6) Lewerenz, M.; Quack, M. Vibrational Spectrum and Potential Energy Surface of the CH Chromophore in CHD_3. *J. Chem. Phys.* **1988**, *88*, 5408−5432.

(7) Marquardt, R.; Quack, M. Global Analytical Potential Hypersurfaces for Large Amplitude Motion and Reactions in Methane. I. Formulation of the Potentials and Adjustment of the Parameters to ab Initio Data and Experimental Contraints. *J. Chem. Phys.* **1998**, *109*, 10628−10643.

(8) Marquardt, R.; Quack, M. Global Analytical Potential Hypersurfaces for Large Amplitude Motion and Reactions in Methane. II. Characteristic Properties of the Potential and Comparison to Other Potentials and Experimental Information. *J. Phys. Chem. A* **2004**, *108*, 3166−3181.

(9) Kuhn, B.; Rizzo, T. R.; Luckhaus, D.; Quack, M.; Suhm, M. A New Six Dimensional Analytical Potential up to Chemically Significant Energies for the Electronic Ground State of Hydrogen Peroxide. *J. Chem. Phys.* **1999**, *111*, 2565−2587.

(10) Shirin, S. V.; Polyansky, O. L.; Zobov, N. F.; Barletta, P.; Tennyson, J. Spectroscopically Determined Potential Energy Surface of $H_2^{16}O$ up to 25 000 cm^{-1}. *J. Chem. Phys.* **2003**, *118*, 2124−2129.

(11) Quack, M.; Suhm, M. A. Potential Energy Surfaces, Quasiadiabatic Channels, Rovibrational Spectra, and Intramolecular Dynamics of $(HF)_2$ and Its Isotopomers from Quantum Monte Carlo Calculations. *J. Chem. Phys.* **1991**, *95*, 28−59.

(12) Klopper, W.; Quack, M.; Suhm, M. HF Dimer: Empirically Refined Analytical Potential Energy and Dipole Hypersurfaces from ab Initio Calculations. *J. Chem. Phys.* **1998**, *108*, 10096−10115.

(13) Klopper, W.; Quack, M.; Suhm, M. A. A New ab Initio Based Six-Dimensional Semi-Empirical Pair Interaction Potential for HF. *Chem. Phys. Lett.* **1996**, *261*, 35−44.

(14) Rajamäki, T.; Miani, A.; Halonen, L. Vibrational Energy Levels for Symmetric and Asymmetric Isotopomers of Ammonia with an Exact Kinetic Energy Operator and New Potential Energy Surfaces. *J. Chem. Phys.* **2003**, *118*, 6358−6369.

(15) Yurchenko, S. N.; Barber, R. J.; Yachmenev, A.; Thiel, W.; Jensen, P.; Tennyson, J. A Variationally Computed T = 300 K Line List for NH_3. *J. Phys. Chem. A* **2009**, *113*, 11845−11855.

(16) Huang, X.; Schwenke, D. W.; Lee, T. J. Rovibrational Spectra of Ammonia. I. Unprecedented Accuracy of a Potential Energy Surface Used with Nonadiabatic Corrections. *J. Chem. Phys.* **2011**, *134*, 044320.

(17) Yurchenko, S. N.; Barber, R. J.; Tennyson, J.; Thiel, W.; Jensen, P. Towards Efficient Refinement of Molecular Potential Energy Surfaces: Ammonia As a Case Study. *J. Mol. Spectrosc.* **2011**, *268*, 123−129.

(18) Ho, T.-S.; Rabitz, H. Inversion of Experimental Data to Extract Intermolecular and Intramolecular Potentials. *J. Phys. Chem.* **1993**, *97*, 13447−13456.

(19) Althorpe, S. C.; Clary, D. C. Quantum Scattering Calculations on Chemical Reactions. *Annu. Rev. Phys. Chem.* **2003**, *54*, 493−529.

(20) Tennyson, J. *Handbook of High-Resolution Spectroscopy*; John Wiley & Sons, Ltd: New York, 2011; Chapter 19, pp 551−572.

(21) Polyansky, O. L.; Zobov, N. F.; Mizus, I. I.; Lodi, L.; Yurchenko, S. N.; Tennyson, J.; Csaszar, A. G.; Boyarkin, O. V. Global Spectroscopy of the Water Monomer. *Philos. Trans. R. Soc. A* **2012**, *370*, 2728−2748.

(22) Marquardt, R.; Sagui, K.; Klopper, W.; Quack, M. Global Analytical Potential Energy Surface For Large Amplitude Nuclear Motions in Ammonia. *J. Phys. Chem. B* **2005**, *109*, 8439−8451.

(23) Ballester, M. Y.; Varandas, A. J. C. Double Many-Body Expansion Potential Energy Surface for Ground State HSO_2. *Phys. Chem. Chem. Phys.* **2005**, *7*, 2305−2317.

(24) Zou, S.; Bowman, J.; Brown, A. Full-Dimensionality Quantum Calculations of Acetylene-Vinylidene Isomerization. *J. Chem. Phys.* **2003**, *118*, 10012−10023.

(25) Zhang, X.; Zou, S.; Harding, L. B.; Bowman, J. M. A Global ab Initio Potential Energy Surface for Formaldehyde. *J. Phys. Chem. A* **2004**, *108*, 8980−8986.

(26) Jin, Z.; Braams, B. J.; Bowman, J. M. An ab Initio Based Global Potential Energy Surface Describing $CH_5^+ \rightarrow CH_3^+ + H_2$. *J. Phys. Chem. A* **2006**, *110*, 1569−1574.

(27) Shepler, B. C.; Braams, B. J.; Bowman, J. M. "Roaming" Dynamics in CH_3CHO Photodissociation Revealed on a Global Potential Energy Surface. *J. Phys. Chem. A* **2008**, *112*, 9344−9351.

(28) Huang, X.; Braams, B. J.; Bowman, J. M.; Kelly, R. E. A.; Tennyson, J.; Groenenboom, G. C.; van der Avoird, A. New ab Initio Potential Energy Surface and the Vibration-Rotation-Tunneling Levels of $(H_2O)_2$ and $(D_2O)_2$. *J. Chem. Phys.* **2008**, *128*, 034312.

(29) Morse, P. M. Diatomic Molecules According to the Wave Mechanics. II. Vibrational Levels. *Phys. Rev.* **1929**, *34*, 57−64.

(30) Yarkony, D. R. Exploring Molecular Complexity: Conical Intersections and NH_3 Photodissociation. *J. Chem. Phys.* **2004**, *121*, 628−631.

(31) Nangia, S.; Truhlar, D. G. Direct Calculation of Coupled Diabatic Potential-Energy Surfaces for Ammonia and Mapping of a Four-Dimensional Conical Intersection Seam. *J. Chem. Phys.* **2006**, *124*, 124309.

(32) Zhu, X.; Ma, J.; Yarkony, D. R.; Guo, H. Computational Determination of the $\tilde{A}$ State Absorption Spectrum of NH_3 and of ND_3 Using a New Quasi-Diabatic Representation of the $\tilde{X}$ and $\tilde{A}$ States and Full Six-Dimensional Quantum Dynamics. *J. Chem. Phys.* **2012**, *136*, 234301.

(33) Li, Z. H.; Valero, R.; Truhlar, D. G. Improved Direct Diabatization and Coupled Potential Energy Surfaces for the Photodissociation of Ammonia. *Theor. Chem. Acc.* **2007**, *118*, 9−24.

(34) Viel, A.; Eisfeld, W.; Neumann, S.; Domcke, W. Photoionization-Induced Dynamics of Ammonia: ab Initio Potential Energy Surfaces and Time-Dependent Wave Packet Calculations for the Ammonia Cation. *J. Chem. Phys.* **2006**, *124*, 214306.

(35) Li, Y. Q.; Song, Y. Z.; Song, P.; Li, Y. Z.; Ding, Y.; Sun, M. T.; Ma, F. C. Ab Initio-Based Double Many-Body Expansion Potential Energy Surface for the First Excited Triplet State of the Ammonia Molecule. *J. Chem. Phys.* **2012**, *136*, 194705.

(36) Huang, X.; Schwenke, D. W.; Lee, T. J. An Accurate Global Potential Energy Surface, Dipole Moment Surface, and Rovibrational Frequencies for NH_3. *J. Chem. Phys.* **2008**, *129*, 214304.
(37) Lin, H.; Thiel, W.; Yurchenko, S. N.; Carvajal, M.; Jensen, P. Vibrational Energies for NH_3 Based on High Level ab Initio Potential Energy Surfaces. *J. Chem. Phys.* **2002**, *117*, 11265−11276.
(38) Yurchenko, S. N.; Zheng, J.; Lin, H.; Jensen, P.; Thiel, W. Potential-Energy Surface for the Electronic Ground State of NH_3 up to 20 000 cm^{-1} above Equilibrium. *J. Chem. Phys.* **2005**, *123*, 134308.
(39) Yurchenko, S. N.; Carvajal, M.; Jensen, P.; Lin, H.; Zheng, J.; Thiel, W. Rotation-Vibration Motion of Pyramidal XY_3 Molecules Described in the Eckart Frame: Theory and Application to NH_3. *Mol. Phys.* **2005**, *103*, 359−378.
(40) Yurchenko, S. N.; Carvajal, M.; Lin, H.; Zheng, J.; Thiel, W.; Jensen, P. Dipole Moment and Rovibrational Intensities in the Electronic Ground State of NH_3: Bridging the Gap between ab Initio Theory and Spectroscopic Experiment. *J. Chem. Phys.* **2005**, *122*, 104317.
(41) Leonard, C.; Handy, N. C.; Carter, S. The Barrier to Inversion of Ammonia. *Chem. Phys. Lett.* **2003**, *370*, 360−365.
(42) Snels, M.; Horká-Zelenková, V.; Hollenstein, H.; Quack, M. High-Resolution FTIR and Diode Laser Spectroscopy of Supersonic Jets. In *Handbook of High-Resolution Spectroscopy*; John Wiley & Sons, Ltd: New York, 2011; Chapter 44, pp 1021−1067.
(43) Huang, X.; Schwenke, D. W.; Lee, T. J. Rovibrational Spectra of Ammonia. II. Detailed Analysis, Comparison, and Prediction of Spectroscopic Assignments for $^{14}NH_3$, $^{15}NH_3$, and $^{14}ND_3$. *J. Chem. Phys.* **2011**, *134*, 044321.
(44) Amos, R. D.; et al. *MOLPRO*, version 2002.3, 2002.
(45) Kendall, R. A.; Dunning, T. H., Jr.; Harrison, R. J. Electron Affinities of the First Row Atoms Revisited. Systematic Basis Sets and Wave Functions. *J. Chem. Phys.* **1992**, *96*, 6796−6806.
(46) Dunning, T. H., Jr. Gaussian Basis Sets for Use in Correlated Molecular Calculations. I. The Atoms Boron through Neon and Hydrogen. *J. Chem. Phys.* **1989**, *90*, 1007.
(47) Langhoff, S. R.; Davidson, E. R. Configuration Interaction Calculations on the Nitrogen Molecule. *Int. J. Quantum Chem.* **1974**, *8*, 61−72.
(48) Werner, H.-J.; Knowles, P. An Efficient Internally Contracted Multiconfiguration-Reference Configuration Interaction Method. *J. Chem. Phys.* **1988**, *89*, 5803−5814.
(49) Knowles, P.; Werner, H.-J. An Efficient Method for the Evaluation of Coupling Coefficients in Configuration Interaction Calculations. *Chem. Phys. Lett.* **1988**, *145*, 514−522.
(50) Berkowitz, J.; Ellison, G. B.; Gutman, D. Three Methods to Measure RH Bond Energies. *J. Phys. Chem.* **1994**, *98*, 2744−2765.
(51) Luckhaus, D. 6D Vibrational Quantum Dynamics: Generalized Coordinate Discrete Variable Representation and (A)Diabatic Contraction. *J. Chem. Phys.* **2000**, *113*, 1329−1347.
(52) Meyer, R.; Günthard, H. H. General Internal Motion in Molecules, Classical and Quantum−Mechanical Hamiltonian. *J. Chem. Phys.* **1968**, *49*, 1510−1520.
(53) Wei, H. Ghost Levels and Near-Variational Forms of the Discrete Variable Representation: Application to H_2O. *J. Chem. Phys.* **1997**, *106*, 6885−6900.
(54) Carrington, T. Using Iterative Methods to Compute Vibrational Spectra. In *Handbook of High-Resolution Spectroscopy*; John Wiley & Sons, Ltd: New York, 2011; Chapter 18, pp 572−586.
(55) Marquardt, R.; Quack, M.; Thanopoulos, I.; Luckhaus, D. A Global Electric Dipole Function of Ammonia and Isotopomers in the Electronic Ground State. *J. Chem. Phys.* **2003**, *119*, 10724−10732.
(56) Dymarsky, A. Y.; Kudin, K. N. Computation of the Pseudorotation Matrix to Satisfy the Eckart Axis Conditions. *J. Chem. Phys.* **2005**, *122*, 124103.
(57) Carter, S.; Bowman, J.; Handy, N. C. Extensions and Tests of "Multimode": a Code to Obtain Accurate Vibration/Rotation Energies of Many-Mode Molecules. *Theor. Chem. Acc.* **1998**, *100*, 191−198.
(58) Yurchenko, S. N.; Thiel, W.; Jensen, P. Theoretical {ROVibrational} Energies (TROVE): A Robust Numerical Approach to the Calculation of Rovibrational Energies for Polyatomic Molecules. *J. Mol. Spectrosc.* **2007**, *245*, 126−140.
(59) Hougen, T.; Bunker, P. R.; Johns, J. W. C. The Vibration-Rotation Problem in Triatomic Molecules Allowing for a Large-Amplitude Bending Vibration. *J. Mol. Spectrosc.* **1970**, *34*, 136−172.
(60) Cooley, J. W. An Improved Eigenvalue Corrector Formula for Solving the Schrödinger Equation for Central Fields. *Math. Comput.* **1961**, *15*, 363−374.
(61) Ovsyannikov, R. I.; Thiel, W.; Yurchenko, S. N.; Carvajal, M.; Jensen, P. Vibrational Energies of PH_3 Calculated Variationally at the Complete Basis Set Limit. *J. Chem. Phys.* **2008**, *129*, 044309.
(62) Marquardt, R. Non Linear Adjustments with External Conditions. *J. Math. Chem.* **2012**, *50*, 577−587.
(63) Gabriel, W.; Chambaud, G.; Rosmus, P.; Carter, S.; Handy, N. C. Theoretical Study of the Renner-Teller $\tilde{A}^2A_1-\tilde{X}^2B_1$ System of NH_2. *Mol. Phys.* **1994**, *81*, 1445−1461.
(64) Martin, J. M. L. Spectroscopic Quality ab Initio Potential Curves for CH, NH, OH and HF. A Convergence Study. *Chem. Phys. Lett.* **1998**, *292*, 411−420.
(65) Herzberg, G. *Molecular Spectra and Molecular Structure I. Spectra of Diatomic Molecules* (reprint 1989); Van Nostrand Reinhold Co.: New York, 1945.
(66) Klopper, W.; Samson, C. C. M.; Tarczay, G.; Császár, A. G. Equilibrium Inversion Barrier of NH_3 from Extrapolated Coupled-Cluster Pair Energies. *J. Comput. Chem.* **2001**, *22*, 1306−1314.
(67) Helgaker, T.; Gauss, J.; Jørgensen, P.; Olsen, J. The Prediction of Molecular Equilibrium Structures by the Standard Electronic Wave Functions. *J. Chem. Phys.* **1997**, *106*, 6430−6440.
(68) Gray, D. L.; Robiette, A. G. The Anharmonic Force Field and Equilibrium Structure of Methane. *Mol. Phys.* **1979**, *37*, 1901−1920.
(69) Benedict, W. S.; Plyler, E. K. Vibration-Rotation Bands of Ammonia. *Can. J. Phys.* **1957**, *35*, 1235−1241.
(70) Pawlowski, F.; Jørgensen, P.; Olsen, J.; Hegelund, F.; Helgaker, T.; Gauss, J.; Bak, K. L. Molecular Equilibrium Structures from Experimental Rotational Constants and Calculated Vibration-Interaction Constants. *J. Chem. Phys.* **2002**, *116*, 6482.
(71) Longuet Higgins, H. C. The Symmetry Groups of Non-Rigid Molecules. *Mol. Phys.* **1963**, *6*, 445.
(72) Quack, M. Fundamental Symmetries and Symmetry Violations from High-Resolution Spectroscopy. In *Handbook of High-Resolution Spectroscopy*; John Wiley & Sons, Ltd: New York, 2011; pp 659−722.
(73) Cohen, E. R.; Cvitas, T.; Frey, J. G.; Holmström, B.; Kuchitsu, K.; Marquardt, R.; Mills, I.; Pavese, F.; Quack, M.; Stohner, J.; Strauss, H. L.; Takami, M.; Thor, A. J. *Quantities, Units and Symbols in Physical Chemistry*, 3rd ed.; Royal Society of Chemistry: Cambridge, U.K., 2007.
(74) Ben Amor, N.; Ambrosek, D.; Daniel, C.; Marquardt, R. The Photodissociation of Trimethyltiniodide. *Chem. Phys.* **2007**, *338*, 81−89.
(75) Chase, M. W., Jr.; Davies, C. A.; Downey, J. R., Jr.; Frurip, D. J.; McDonald, R. A.; Syverud, A. N. *JANAF Thermochemical Tables*, 3rd ed.; American Chemical Society and American Institute of Physics for the National Bureau of Standards: Washington, DC, 1985; Vol. *14*, Suppl. 1.
(76) Xu, Z.-F.; Fang, D.-C.; Fu, X.-Y. Theoretical Studies on the Dynamical Properties of the Reaction $NH_2 + H \rightarrow NH + H_2$. *J. Phys. Chem.* **1995**, *99*, 5889−5893.
(77) Herzberg, G. *Molecular Spectra and Molecular Structure II. Infrared and Raman Spectra of Polyatomic Molecules*, (reprint 1991); Van Nostrand Reinhold Co.: New York, 1945.
(78) Joint Commission for Spectroscopy from IAU and IUPAP. Report on Notation for the Spectra of Polyatomic Molecules. *J. Chem. Phys.* **1955**, *23*, 1997−2011.
(79) Merkt, F.; Quack, M. Molecular Quantum Mechanics and Molecular Spectra, Molecular Symmetry and Interaction of Matter with Radiation. In *Handbook of High-Resolution Spectroscopy*; John Wiley & Sons, Ltd: New York, 2011; Chapter 1, pp 1−56.
(80) Lai, W.; Lin, S. Y.; Xie, D.; Guo, H. Full-Dimensional Quantum Dynamics of Ã-State Photodissociation of Ammonia: Absorption Spectra. *J. Chem. Phys.* **2008**, *129*, 154311.
(81) Sung, K.; Brown, L. R.; Huang, X.; Schwenke, D. W.; Lee, T. J.; Coy, S. L.; Lehmann, K. K. Extended Line Positions, Intensities,

Empirical Lower State Energies and Quantum Assignments of NH_3 from 6300 to 7000 cm^{-1}. *J. Quant. Spectrosc. Radiat. Transfer* **2012**, *113*, 1066−1083.
(82) Coy, S. L.; Lehmann, K. K. Modeling the Rotational and Vibrational Structure of the I.R. and Optical Spectrum of NH_3. *Spectrochim. Acta* **1989**, *45A*, 47−56.
(83) Kleiner, I.; Brown, L. R.; Tarrago, G.; Kou, Q.-L.; Picqué, N.; Guelachvili, G.; Dana, V.; Mandin, J.-Y. Positions and Intensities in the $2\nu_4/\nu_1/\nu_3$ Vibrational System of $^{14}NH_3$ near 3 μm. *J. Mol. Spectrosc.* **1999**, *193*, 46−71.
(84) Špirko, V.; Kraemer, W. P. Anharmonic Potential Function and Effective Geometries for the NH_3 Molecule. *J. Mol. Spectrosc.* **1989**, *133*, 331−344.
(85) Berden, G.; Peeters, R.; Meijer, G. Cavity-Enhanced Absorption Spectroscopy of the 1.5 μm Band System of Jet-Cooled Ammonia. *Chem. Phys. Lett.* **1999**, *307*, 131−138.
(86) Xu, L.-H.; Liu, Z.; Yakovlev, I.; Tretyakov, M. Y.; Lees, R. M. External Cavity Tunable Diode Laser NH_3 Spectra in the 1.5 μm Region. *Infrared Phys. Technol.* **2004**, *45*, 31−45.
(87) Lees, R. M.; Li, L.; Xu, L.-H. New VISTA on Ammonia in the 1.5 μm Region: Assignments for the $\nu_3 + 2\nu_4$ Bands of $^{14}NH_3$ and $^{15}NH_3$ by Isotopic Shift Labeling. *J. Mol. Spectrosc.* **2008**, *251*, 241−251.
(88) Snels, M.; Hollenstein, H.; Quack, M. The NH and ND Stretching Fundamentals of $^{14}ND_2H$. *J. Chem. Phys.* **2003**, *119*, 7993−7902.
(89) Snels, M.; Hollenstein, H.; Quack, M. The NH and ND Stretching Fundamentals of $^{14}NH_2D$. *J. Mol. Spectrosc.* **2006**, *237*, 143−148.
(90) Marquardt, R.; Quack, M.; Thanopoulos, I.; Luckhaus, D. Tunneling Motion of the Infrared NH Chromophore in NHD_2 During and After Coherent Excitation. *J. Chem. Phys.* **2003**, *118*, 643−658.
(91) Marquardt, R.; Sanrey, M.; Gatti, F.; Quéré, L. Full-Dimensional Quantum Dynamics of Vibrationally Highly Excited NHD_2. *J. Chem. Phys.* **2010**, *133*, 174302.
(92) Cuvelier, F.; Hervé, S.; Marquardt, R.; Sagui, K. Potential Energy Surfaces for Vibrational and Rotational Wave Packet Motion in Polyatomic Molecular Systems. *CHIMIA* **2004**, *58*, 296−305.
(93) Urban, Š.; Špirko, V.; Papoušek, D.; Kauppinen, J.; Belov, S. B.; Gershtein, L. I.; Krupnov, A. F. A Simultaneous Analysis of the Microwave, Submillimeterwave, Far Infrared, and Infrared-Microwave Two-Photon Transitions between the Ground and ν_2 Inversion-Rotation Levels of $^{14}NH_3$. *J. Mol. Spectrosc.* **1981**, *88*, 274−292.
(94) Tanaka, K.; Ito, H.; Tanaka, T. CO_2 Laser-Microwave Double Resonance Spectroscopy of NH_3: Precise Measurement of Dipole Moment in the Ground State. *J. Chem. Phys.* **1987**, *87*, 1557−1567.
(95) Urban, Š.; Papoušek, D.; Devi, V. M.; Fridovich, B.; D'Cunha, R.; Rao, K. N. Transition Dipole Matrix Elements for $^14NH_3$ from the Line Intensities of the $2\nu_2$ and ν_4 Bands. *J. Mol. Spectrosc.* **1984**, *86*, 38−55.
(96) Cottaz, C.; Kleiner, I.; Tarrago, G.; Brown, L. R.; Margolis, J. S.; Poynter, R. L.; Pickett, H. M.; Fourchet, T.; Drossart, P.; Lellouch, E. Line Positions and Intensities in the $2\nu_2/\nu_4$ Vibrational System of $^{14}NH_3$ near 5−7 μm. *J. Mol. Spectrosc.* **2000**, *203*, 285−309.
(97) Kleiner, I.; Tarrago, G.; Brown, L. R. Positions and Intensities in the $3\nu_2/\nu_2 + \nu_4$ Vibrational System of $^{14}NH_3$ near 4 μm. *J. Mol. Spectrosc.* **1995**, *173*, 120−145.
(98) Guelachvili, G.; Abdullah, A. H.; Tu, N.; Rao, K. N.; Urban, Š.; Papoušek, D. Analysis of High-Resolution Fourier Transform Spectra of $^{14}NH_3$ at 3.0 μm. *J. Mol. Spectrosc.* **1989**, *133*, 345−364.
(99) Cottaz, C.; Kleiner, I.; Tarrago, G.; Brown, L. R. Assignments and Intensities of $^{14}NH_3$ Hot Bands in the 5- to 8- μm ($3\nu_2 - \nu_2,\nu_2 + \nu_4 - \nu_2$) and 4- μm ($4\nu_2 - \nu_2,\nu_1 - \nu_2,\nu_3 - \nu_2$ and $2\nu_4 - \nu_2$) Regions. *J. Mol. Spectrosc.* **2001**, *209*, 30−49.
(100) Ziegler, L. D.; Hudson, B. Resonance Rovibronic Raman Scattering of Ammonia. *J. Phys. Chem.* **1984**, *88*, 1110−1116.
(101) Urban, Š.; Tu, N.; Rao, K. N.; Guelachvili, G. Analysis of High-Resolution Fourier Transform Spectra of $^{14}NH_3$ at 2.3 μm. *J. Mol. Spectrosc.* **1989**, *133*, 312−330.
(102) Margolis, J. S.; Kwan, Y. Y. The Measurement of the Absorption Strengths of Some Lines in the $\nu_1 + \nu_2$ and $\nu_2 + \nu_3$ Bands of Ammonia. *J. Mol. Spectrosc.* **1974**, *50*, 266−280.
(103) Coudert, L.; Valentin, A.; Henry, L. Inversion Doubling in the ν_2 Vibration-Rotation Band of NH_2D and ND_2H. *J. Mol. Spectrosc.* **1986**, *120*, 185−204.
(104) Kartha, S. B.; Singh, K.; Job, V. A.; Kartha, V. B. Transition Dipole Moments and Refined Molecular Parameters for the ν_2 Band of ND_2H. *J. Mol. Spectrosc.* **1988**, *129*, 86−98.
(105) Fusina, L.; Di Leonardo, G.; Johns, J. W. C. The ν_2 and ν_4 Bands of $^{14}ND_3$. *J. Mol. Spectrosc.* **1986**, *118*, 397−423.
(106) Snels, M.; Fusina, L.; Hollenstein, H.; Quack, M. The ν_1 and ν_3 Band of ND_3. *Mol. Phys.* **2000**, *98*, 837−854.
(107) Coon, J. B.; Naugle, N. W.; McKenzie, R. D. The Investigation of Double-Minimum Potentials in Molecules. *J. Mol. Spectrosc.* **1966**, 107−129.
(108) Snels, M.; Hollenstein, H.; Quack, M. Mode Selective Tunneling Dynamics Observed by High Resolution Spectroscopy of the Bending Fundamentals of $^{14}NH_2D$ and $^{14}ND_2H$. *J. Chem. Phys.* **2006**, *125*, 194319.